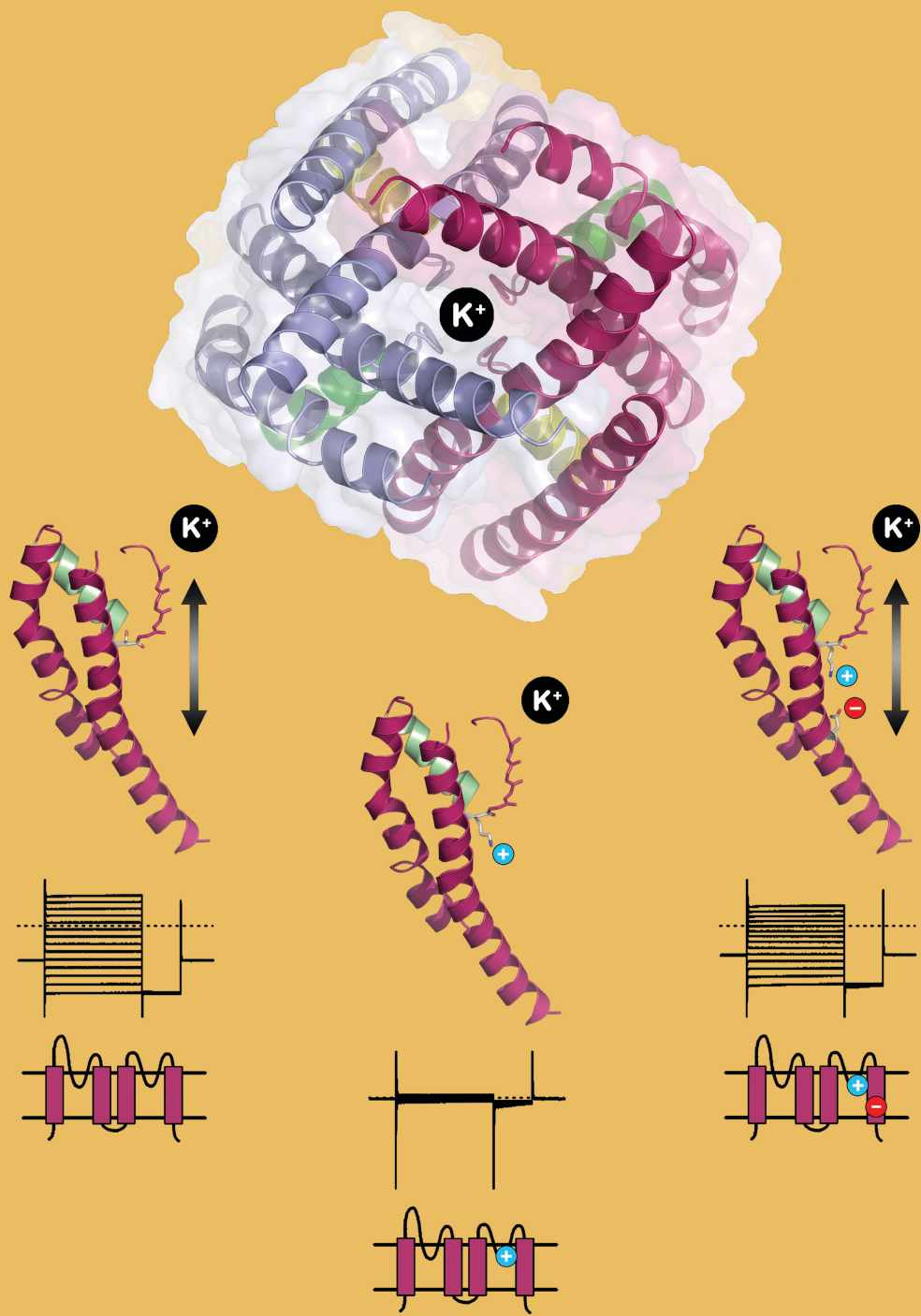


JGP

The Journal of General Physiology

Vol 134 • No 1 • July 2009



A structural model for $K_{2P}\emptyset$ potassium channels based on 23 pairs of interacting sites and continuum electrostatics

Astrid Kollewe,¹ Albert Y. Lau,² Ashley Sullivan,¹ Benoît Roux,² and Steve A.N. Goldstein¹

¹Institute for Molecular Pediatric Sciences, Department of Pediatrics, and ²Department of Biochemistry and Molecular Biology, The University of Chicago, Pritzker School of Medicine, Chicago, IL 60637

$K_{2P}\emptyset$, the two-pore domain potassium background channel that determines cardiac rhythm in *Drosophila melanogaster*, and its homologues that establish excitable membrane activity in mammals are of unknown structure. K_{2P} subunits have two pore domains flanked by transmembrane (TM) spans: TM1-P1-TM2-TM3-P2-TM4. To establish spatial relationships in $K_{2P}\emptyset$, we identified pairs of sites that display electrostatic compensation. Channels silenced by the addition of a charge in pore loop 1 (P1) or P2 were restored to function by countercharges at specific second sites. A three-dimensional homology model was determined using the crystal structure of $K_v1.2$, effects of $K_{2P}\emptyset$ mutations to establish alignment, and compensatory charge–charge pairs. The model was refined and validated by continuum electrostatic free energy calculations and covalent linkage of introduced cysteines. K_{2P} channels use two subunits arranged so that the P1 and P2 loops contribute to one pore, identical P loops face each other diagonally across the pore, and the channel complex has bilateral symmetry with a fourfold symmetric selectivity filter.

INTRODUCTION

K_{2P} potassium channel subunits in animals have two pore (P) loop domains and four transmembrane (TM) segments (Ketchum et al., 1995; Goldstein et al., 1996, 2001; Lesage et al., 1996; Thomas et al., 2008). Expressed ubiquitously, these background channels modulate the excitable activity of membranes because they operate at resting membrane potentials (Goldstein et al., 1996; Duprat et al., 1997; Lopes et al., 2000). K_{2P} channel function is tightly regulated by a plethora of natural and medicinal agents (Lotshaw, 2007; Thomas and Goldstein, 2009), and their roles in health and disease are emerging (Mulkey et al., 2007; Bautista et al., 2008; Davies et al., 2008).

Potassium channels of known structure are symmetric assemblies of four pore-forming subunits, each contributing one P loop and flanking TM spans (TM-P-TM) to a single, central, ion-selective pathway (Doyle et al., 1998; Jiang et al., 2002, 2003; Kuo et al., 2003; Long et al., 2005). Because K_{2P} subunits have two such modules linked in series, TM1-P1-TM2-TM3-P2-TM4, it was expected that two subunits would be necessary and sufficient to form functional channels. Indeed, a dimeric stoichiometry has been inferred for $K_{2P}3$ (Lopes et al., 2001; Yuill et al., 2007) and $K_{2P}5$ (Niemeyer et al., 2007) based on the functional effects of point mutations.

In this study, we sought to generate a three-dimensional model for $K_{2P}\emptyset$, the well-characterized K_{2P} channel of *Drosophila melanogaster* excitable tissues (Goldstein et al., 1996; Zilberberg et al., 2000, 2001; Ilan and Goldstein,

2001; Ben-Abu et al., 2009) that determines cardiac rhythm in the fly (Lalevée et al., 2006). The purpose was to confirm the contribution of both P1 and P2 and just two subunits to the formation of a single pore and to design, evaluate, and refine a structural model using known potassium channel crystal structures, molecular dynamics (MD; Roux and Schulten, 2004), and experimental constraints determined as follows.

Our strategy is based on the discovery of Chatelain et al. (2005) that suppression of ion conduction by addition of a charged residue in the P loop of $K_{IR}2.1$ can be reversed by introduction of a countercharge at specific pore-lining sites in the next TM segment. In the present study, we identify 21 pairs of such compensatory sites in $K_{2P}\emptyset$. Next, $K_{2P}\emptyset$ sites likely to face the pore were identified based on effects of aspartate substitution (Nimigean et al., 2003) and were used to achieve alignment with crystallized potassium channels. The model was refined by comparison of sites showing electrostatic compensation and calculated electrostatic free energies reflecting potassium stability in the pore and cross-linking of two pairs of $K_{2P}\emptyset$ channel sites, one of which was reported previously (Zilberberg et al., 2001). The results demonstrate that two $K_{2P}\emptyset$ subunits fold like single P-loop subunits linked in tandem, forming one ion conduction pathway with two P1 and two P2 loops contributing directly to one pore. The model reveals a complex with bilateral symmetry that has fourfold pseudosymmetry at the potassium selectivity filter.

Correspondence to Steve A.N. Goldstein: sangoldstein@uchicago.edu

Abbreviations used in this paper: DTNB, 5,5'-dithiobis(2-nitrobenzoic acid); DTT, dithiothreitol; MD, molecular dynamics; RMSD, root mean square deviation; TM, transmembrane; WT, wild type.

MATERIALS AND METHODS

Molecular biology

cDNA encoding amino acids 1–298 of $K_{2p}\emptyset$ (GenBank/EMBL/DDBJ accession no. U55321) was subcloned into pRAT, a dual expression vector based on PCR3.1 and pGEM with T7 and cytomegalovirus promoters. For detection in Western blots, nucleotides encoding a 1D4 tag (ARVPDGDPDETSQVAPA) were inserted before the stop codon. To generate tandem $K_{2p}\emptyset$ constructs, a BstXI restriction site was inserted between the two genes, creating a five-amino acid linker (ASGVA) at residue 298 of the first subunit and the initiation methionine of the second. Mutations were introduced by PCR and confirmed by DNA sequencing. cRNA was synthesized with T7 polymerase using an mMessageMachine kit (Applied Biosystems), and yield was determined by spectrophotometry.

Electrophysiology

Oocytes were extracted from *Xenopus laevis* and defolliculated with collagenase type 2 (Worthington). Oocytes were maintained in 83-mM KCl solution: 83 mM KCl, 10 mM NaCl, 1 mM MgCl₂, 1.8 mM CaCl₂, and 5 mM HEPES, pH 7.5, with NaOH supplemented with 1% penicillin/streptomycin (Cellgro) and 0.1% gentamycin sulfate (Invitrogen). Currents were recorded 1–3 d after injection of 0.5–25 ng cRNA. Perfusion solution for two electrode voltage-clamp recordings contained 100 mM KCl, 1 mM MgCl₂, 0.3 mM CaCl₂, and 5 mM HEPES, pH 7.5, with NaOH. The current protocol was (a) a holding voltage of −77 mV, (b) 250-ms steps of 15 mV from −135 to 60 mV, and (c) a 100-ms step to −135 mV every 2 s. To confirm that nonspecific leak was not confounding, measurements were first made with 5 mM bath KCl while holding at −77 mV (the reversal potential under these conditions) before switching to 100-K solution. For experiments with dithiothreitol (DTT) or 5,5'-dithiobis(2-nitrobenzoic acid) (DTNB), oocytes were maintained in 83-mM KCl solution supplemented with 100 μM DTT, and currents recorded during a 250-ms pulse to 30 mV from a holding voltage of −77 mV followed by a 100-ms step to −135 mV were collected every 2 s. The perfusion solution contained 5 mM KCl, 95 mM NaCl, 1 mM MgCl₂, 0.3 mM CaCl₂, and 5 mM HEPES, pH 7.5, with NaOH.

Two-electrode voltage-clamp data acquisition was performed with an oocyte clamp (OC-725B; Warner Instruments Corp.) at a sampling rate of 1–5 kHz. Data were processed using pCLAMP (MDS Analytical Technologies), IGOR Pro (WaveMetrics), and Microsoft Office Excel (Microsoft) software. Single-channel recordings were performed by patch-clamp technique in on-cell mode using an amplifier (EPC-9; HEKA) and Pulse+PulseFit 8.02 software and were recorded to videotape. Single-channel amplitudes were determined from all-points histograms after sampling at 20 kHz and filtering at 5 kHz using pCLAMP software. Bath and pipette solution contained 140 mM KCl, 2 mM MgCl₂, 5 mM EGTA, and 5 mM HEPES, pH 7.4, with NaOH. All experiments were performed at room temperature.

Although two S104K or T216K substitutions (in monomer or tandem subunits) fully suppressed current, tandem channels with one suppressive lysine in the four P loops showed reduced flux; to avoid variable restoration with second site mutations seen with longer incubation times, tandem channels were studied 24 h after cRNA injection.

Statistical analysis

The significance of the difference between two data points was determined with a *t* test and is indicated as follows: *, P < 0.05; **, P < 0.01; ***, P < 0.001.

Biochemistry

200–250 oocytes were injected with 15 ng cRNA and incubated for 2 d in 83-mM KCl solution. Cell surface proteins were biotinylated by 2-h incubation with 0.7 mg/ml EZ-Link sulfo-NHS-SS-biotin (Thermo Fisher Scientific) in ND91 (2 mM KCl, 91 mM NaCl,

1 mM MgCl₂, 1.8 mM CaCl₂, and 5 mM HEPES, pH 7.5, with NaOH at room temperature). Nonreacted reagent was quenched with 50 mM Tris, pH 8.0, with HCl, and cells were lysed in a glass homogenizer in 2 ml of lysis buffer: 40 mM KCl, 0.1 mM NaCl, 1 mM EDTA, 20 mM HEPES, pH 7.4, with NaOH, 10% glycerol, 1% CHAPS (Thermo Fisher Scientific), and EDTA-free complete protease inhibitor cocktail tablets (Roche). Total soluble proteins were isolated after incubation with agitation for 90 min at 4°C and removal of lipids and cell debris by three cycles of centrifugation for 5 min at 5,000 g. To isolate biotinylated cell surface proteins, the total soluble protein was incubated with streptavidin immobilized on beads (Thermo Fisher Scientific) for 2 h at 4°C, three washes of the beads, and elution of bound protein by incubation at 95°C in SDS-PAGE sample buffer supplemented with 50 mM DTT.

Proteins were separated by SDS-PAGE on a 8–16% gel (Bio-Rad Laboratories) and transferred onto nitrocellulose membranes, and $\Delta K_{2p}\emptyset$ was stained with a monoclonal mouse anti-1D4 antibody to the epitope ETSQVAPA (National Cell Culture Center) followed by Alexa Fluor 680 coupled to a goat anti–mouse antibody (Invitrogen). Visualization was conducted with a scanner (Odyssey; LI-COR Biosciences).

Homology modeling

$K_{v1.2}$ (PDB accession no. 2A79) was used as the primary structural template. To align $K_{2p}\emptyset$ and $K_{v1.2}$, multiple sequence alignment was performed using the program ClustalW (Higgins et al., 1996) with K_vAP , $KcsA$, $K_{v}Bac1.1$, and $MthK$ (Doyle et al., 1998; Jiang et al., 2002, 2003; Kuo et al., 2003). Neither insertions nor deletions were allowed within known helical segments of $K_{v1.2}$. First, the alignment was constructed using both $K_{2p}\emptyset$ channel domains simultaneously along with secondary structure constraints. The resulting $K_{2p}\emptyset$ model was incompatible with experimentally determined pore access of four of nine residues in TM4 and rescue by two residues in TM4. Therefore, TM1–TM2 and TM3–TM4 were separately aligned with the other channels; the outcome was full alignment of pore-exposed residues in crystallized potassium channels and $K_{2p}\emptyset$ (Fig. S5).

Once the alignment was established, a peptide sequence for MD was designed by joining two subunits of $K_{v1.2}$ to reflect the arrangement in a single $K_{2p}\emptyset$ subunit. Helices TM2 and TM3 of $K_{2p}\emptyset$ were joined with clockwise rotation as viewed from the outside of the channel. Polypeptide insertions were built using ModLoop (Fiser and Sali, 2003). Side chain substitution was performed using SCWRL (Canutescu et al., 2003). Restrained energy minimization and MD were performed using the program CHARMM (Brooks et al., 1983) and the all-atom potential energy function for proteins, PARAM22 (MacKerell et al., 1998). The deviation between the two subunits was minimized using a root mean square deviation (RMSD) biasing potential with MD and energy minimization. Special attention was paid to the helical segments flanking P131, P183, and P192 to allow proline-induced distortions to form (see A model for $K_{2p}\emptyset$ adopts bilateral symmetry). Omitted from the model were highly flexible regions that could not be predicted with confidence: the TM1–P1 linker of $K_{2p}\emptyset$ (a segment 53 amino acids longer than in $K_{v1.2}$), the TM2–TM3 linker, and the P2–TM4 segment.

All continuum electrostatic calculations were based on the finite difference Poisson-Boltzmann equation (Honig and Nicholls, 1995; Roux and MacKinnon, 1999; Roux et al., 2000), as these provide a qualitative assessment of how residue substitutions affect ion transport through the channel. In these calculations, the hydrocarbon core of the membrane is represented as a uniform slab 25 Å thick with a dielectric constant of 2 (White and Wiener, 1996). A dielectric constant of 4 was used for the protein interior (King et al., 1991; Simonson and Perahia, 1995; Simonson and Brooks, 1996). A cylinder of 12-Å radius and a dielectric constant of 80 was cut from the membrane slab before the channel structure was

overlaid onto it in order to assign the dielectric constant to the interior of the pore. All Poisson-Boltzmann calculations were performed using the PBEQ module (Nina et al., 1997; Roux, 1997; Im et al., 1998) of CHARMM (Brooks et al., 1983) with the PARAM22 force field (MacKerell et al., 1998). The atomic radii used to define the protein–solvent dielectric boundary were optimized to reproduce the results of MD free energy perturbation calculations using explicit water molecules for the 20 standard amino acids (Nina et al., 1997).

For mutation analysis, residue substitutions were generated using SCWRL, and restrained energy minimization and MD were performed to relax these residues using CHARMM. Shifts in pK_a for these residues were determined by evaluating the reversible work needed to protonate a given side chain in the protein compared with the work needed to protonate the same side chain in an isolated peptide in bulk water (Bashford and Karplus, 1990; Antosiewicz et al., 1996; Roux et al., 2000). This reversible work corresponds to the free energy difference, $\Delta\Delta G$, between the protonated and unprotonated states of an amino acid either embedded in the protein or isolated in bulk solvent. pK_a values used for lysine, aspartate, and glutamate in bulk water are 10.79, 3.90, and 4.07, respectively. pK_a shifts for S104K and T216K mutants were determined in the presence of potassium ions in positions S1 and S3. pK_a shifts for S104E mutants were determined with an additional cavity ion. The protonation states of substituted residues were then used to calculate the static field contribution to the electrostatic free energy barrier for a cation passing through the channel (Jogini and Roux, 2005). To assess the impact of charged mutations on ion permeation, only the static field contribution to the electrostatic free energy barrier was evaluated (Jogini and Roux, 2005); impact was estimated from $\max(|\Delta G_{\text{mut}} - \Delta G_{\text{WT}}|)$, which provides a measure of the dominant free energy barrier (see Fig. 7 E). $\Delta\Delta G$ was computed using the PBEQ module of CHARMM with the same continuum parameters described for the continuum electrostatic calculations. Atomic charges were turned off in these positions: loop regions 30–91, 153–173, 225–238, side chain and carbonyls of 105 and 217 at the bottom of the filter, and the main chain of 106–109 and 218–221 of the filter. Before refinement, calculations were discrepant for 7/57 mutants (Fig. S11). Increasing the distance between L257 residues via energy minimization with a harmonic biasing potential produced correlation for four more mutants and widened the inner cavity. This changed the relative position of main chain atoms by an RMSD of 1.4 Å.

Online supplemental material

Fig. S1 shows silencing of full-length $K_{2P}\emptyset$ by a lysine at S104 or T216 and restoration of current by aspartate substitution in TM2 or TM4. Fig. S2 compares current phenotype, selectivity, and rectification attributes of $K_{2P}\emptyset$ channels formed by monomeric and tandem dimer subunits. Fig. S3 shows that all four P loops contribute to pore formation in channels built with tandem dimer subunits. Fig. S4 demonstrates the impact of single aspartate substitutions in TM2 or TM4 on channel function. Fig. S5 shows the alignment of $K_{2P}\emptyset$ with crystallized potassium channels based on residues found in experiments to be pore exposed. Residues studied in this work are highlighted in the alignment. Fig. S6 provides data for all mutants not shown in Fig. 7 to reveal the relationship between effectiveness of rescue and distance between charged residues and compares calculated changes in $\Delta\Delta G$ with experimentally observed rescue. Fig. S7 schematically illustrates the mechanism of electrostatic compensation. Fig. S8 shows a comparison of experimentally observed rescue with changes in $\Delta\Delta G$ calculated for a fourfold symmetric channel model. Fig. S9 shows the position of residue G139D in a crevice with limited access to the aqueous pore (a site from which it cannot restore current through an electrostatic mechanism). Fig. S10 shows a cross section through

the model of $K_{2P}\emptyset$ and crystallized potassium channels ~4 Å below the selectivity filter. Fig. S11 shows observed current restoration and $\Delta\Delta G$ values calculated for the two-dimensional model of $K_{2P}\emptyset$ before refinement. Main chain coordinates of the model are also included. Online supplemental material is available at <http://www.jgp.org/cgi/content/full/jgp.200910235/DC1>.

RESULTS

A basic residue in P1 or P2 disrupts ion conduction

We follow the strategy of Chatelain et al. (2005), who studied the relationship of residues in the P loop and following TM segment (TM2) in $K_{IR}2.1$ channels (Fig. 1, A and B); they found that substitution of a positively charged lysine for threonine (T141K) was tolerated in the P-loop domain ($T^{141}TIGYG$; Fig. 1, A–C, yellow circles) so long as a naturally occurring aspartate in TM2 was present (D172; Fig. 1, A–C, green circles). Ion flux was lost if D172 was neutralized (D172N) and was restored on subsequent introduction of aspartate at position 169 or 176 (Fig. 1, B and C). Potassium flux despite a lysine in the P loop can be explained by a compensatory through space electrostatic effect of the oppositely charged aspartate (Chatelain et al., 2005; Roux, 2005). This thesis is supported by a model of $K_{IR}2.1$ with positions 169, 172, and 176 exposed in the pore on successive helical turns of TM2 (Fig. 1, C and D). In the $K_{IR}2.1$ model, four subunits each contribute one P loop to the ion selectivity filter, the TM2 segment after each P loop creates the intracellular portion of the ion conduction pathway, and the TM1 segment preceding each P loop forms an investing outer pore helix, as in crystal structures of other potassium channels (Doyle et al., 1998; Jiang et al., 2002, 2003; Kuo et al., 2003; Long et al., 2005).

To evaluate $K_{2P}\emptyset$ by this method, a lysine was introduced into the P loop of domain I (P1; S104K) or the P loop of domain II (P2; T216K), and second site mutations were assessed in nine positions of TM2 (P131–G139) and TM4 (G255–F263). P-loop sites and TM segments were analogous to those studied in $K_{IR}2.1$ (Fig. 1, A and B). We used a $K_{2P}\emptyset$ channel variant lacking amino acids 299–1,000 ($\Delta K_{2P}\emptyset$) to eliminate effects of channel regulation on current amplitude. Whereas $K_{2P}\emptyset$ activity is altered by phosphorylation of the cytoplasmic C terminus (Zilberberg et al., 2000), $\Delta K_{2P}\emptyset$ resembles full-length channels in macroscopic current phenotype, selectivity among monovalent cations, and unitary conductance while displaying a stable open probability of 0.77 (Zilberberg et al., 2000). *Xenopus* oocytes expressing $\Delta K_{2P}\emptyset$ and studied by two-electrode voltage clamp in a bath solution with 100 mM KCl show inward and outward currents that change in magnitude without an apparent delay in response to shifts in membrane voltage (Fig. 2 A) as expected for an open potassium-selective portal and like the full-length channel (Goldstein et al., 1996; Ilan and Goldstein, 2001).

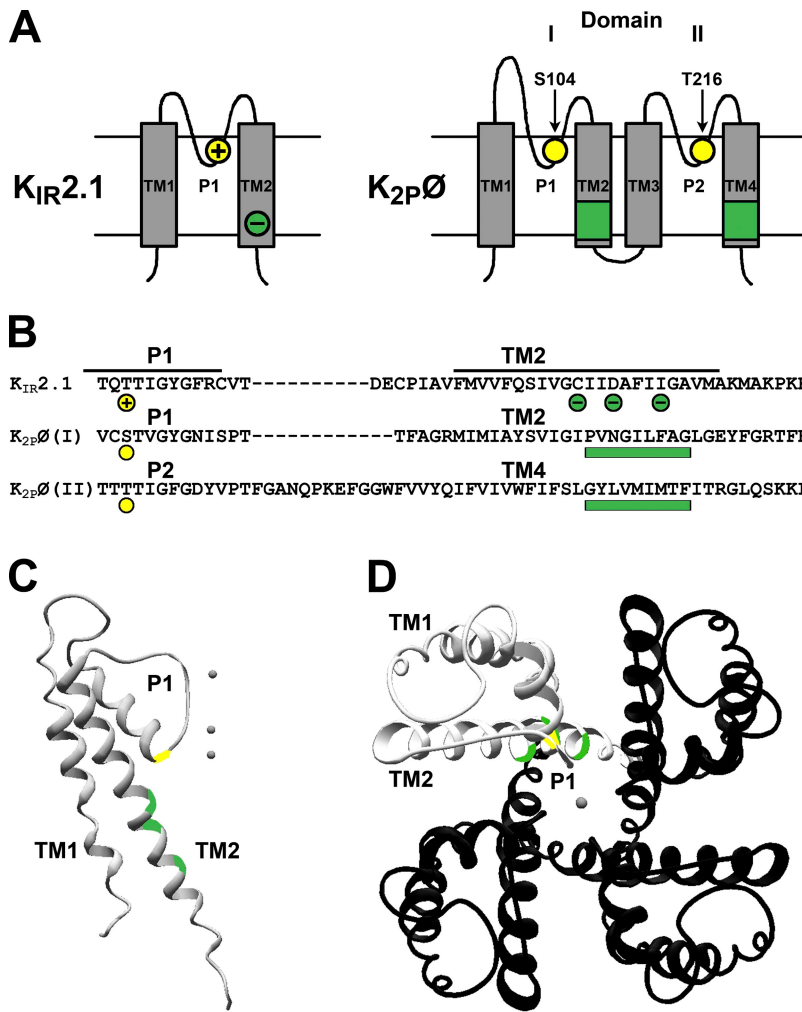


Figure 1. Strategy: identify pairs of sites that show charge-charge compensation. (A, left) Topology of K_{IR}2.1 indicating the P-loop location where lysine suppressed current (T141K; yellow circle) and a site in TM2 where second site mutation to aspartate restored conduction (green circle; Chatelain et al., 2005). (right) Predicted topology of K_{2p}∅ indicating two domains (I and II), two P loops (P1 and P2), and four TM spans (TM1–4). Charged residues at position S104 of P1 or T216 of P2 (yellow circles) and second site changes at P131 to G139 in TM2 or G255 to F263 in TM4 (green boxes) are studied. (B) Alignment of K_{IR}2.1 (amino acids 139–188), K_{2p}∅ P1-TM2 (amino acids 102–149), and K_{2p}∅ P2-TM4 (amino acids 214–273) using ClustalW 1.83. P loops and predicted TM spans are indicated (black lines). The suppressive pore lysine in K_{IR}2.1 (T141K; yellow circle) and complementing aspartate substitutions in TM2 at C169D, D172, or I176D (green circles) as reported by Chatelain et al. (2005) are indicated. K_{2p}∅ positions are highlighted as in A. (C) KcsA subunit noting sites homologous to those in K_{IR}2.1 in A and B. (D) Top view of a KcsA channel with one subunit highlighted as in C.

Potassium flux through ΔK_{2p}∅ channels was suppressed by the substitution of lysine for serine in P1 (S104K; S¹⁰⁴TGTYGN) or for threonine in P2 (T216K; T²¹⁶TIGFGD; Fig. 2 A). The lysine appeared to interfere with ion conduction rather than protein synthesis or surface expression because currents were absent despite injection of large amounts of cRNA (up to 20 ng) or postinjection incubation of oocytes for 4 d. Furthermore, wild-type (WT), S104K, and T216K ΔK_{2p}∅ channels were demonstrated by Western blot analyses to be similarly synthesized (Fig. 2 B, left) and translocated to the oocyte plasma membrane (Fig. 2 B, right) when assessed by cell surface biotinylation.

Second site mutations that restore function in the same domain

ΔK_{2p}∅ channels silenced by lysine in P1 (S104K) were not restored to function by five of nine second site substitutions to aspartate in TM2 of domain I (Fig. 3 A). Four domain I replacements were complementary, restoring ΔK_{2p}∅ channel function; the highest current amplitudes were found for S104K–F137D channels, whereas three other restoring mutations were less potent (N133D,

G134D, and A138D). The four restoring positions in TM2 plot to one face of a helical wheel (Fig. 3 A).

ΔK_{2p}∅ channels silenced by a lysine in P2 (T216K) were unresponsive to five of nine second site substitutions to aspartate in TM4 of domain II. Changes at four other sites restored function: two robustly, L257D and M261D, and two less so, V258D and T262D (Fig. 3 B). The four restoring positions in TM4 plot to one face of a helical wheel (Fig. 3 B).

Second site mutations in the other domain that restore function

If both P loops in a K_{2p}∅ subunit participate in pore formation, it is reasonable to expect that suppression of current by a lysine in P1 at S104 might be complemented not only by an aspartate in TM2 of the same channel domain (Fig. 3 A) but also by second site mutation in TM4, the span following P2 in channel domain II (Fig. 3 C). Indeed, two of nine changes in TM4, V258D and T262D, restored function to S104K channels. Similarly, channels suppressed by a lysine at 216 in P2 recovered their function with a second change to aspartate at three TM2 sites, 134, 138, and 139 (Fig. 3 D).

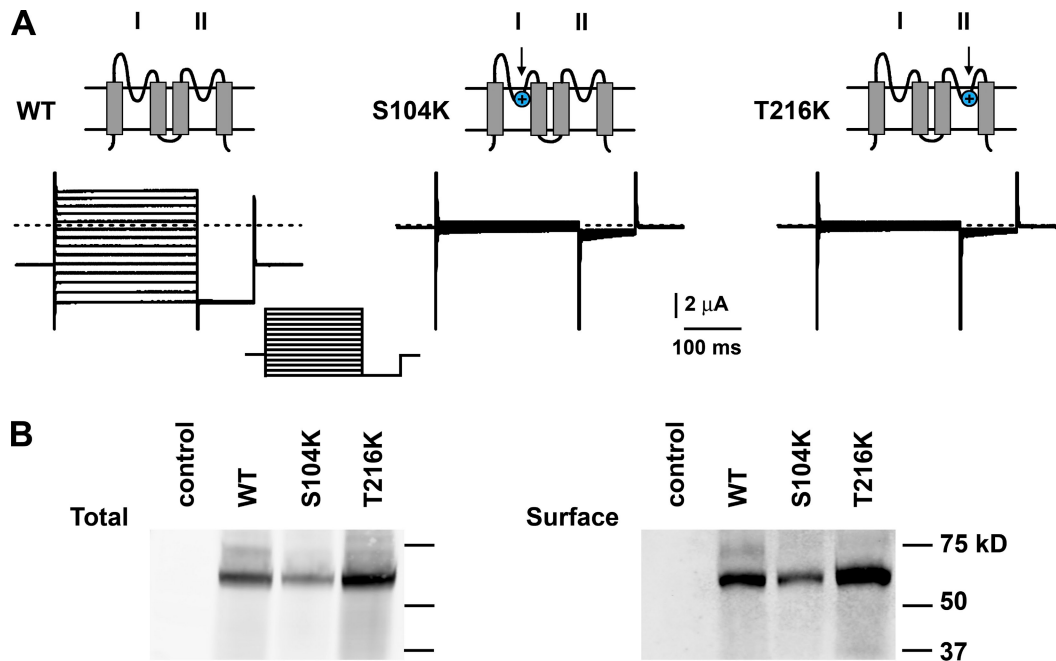


Figure 2. Lysine in P1 or P2 disrupts $\Delta K_{2p}\emptyset$ channel function but not surface expression. Wild-type (WT), S104K, or T216K $\Delta K_{2p}\emptyset$ channels were studied by expression in *Xenopus* oocytes. (A) Sample recordings by two-electrode voltage clamp. The bath solution contained 100 mM KCl (see Materials and methods). Topology insets: blue circles denote S104K in P1 or T216K in P2. Protocol inset: holding voltage of -77 mV with 250-ms steps of 15 mV from -135 to 60 mV followed by a 100-ms step to -135 mV every 2 s. (B) Western blot analyses of channels bearing C-terminal 1D4 tags detected with anti-1D4 antibodies. Channel protein was detected among total soluble protein (left) or surface proteins isolated by biotinylation and purification with streptavidin beads (right) after SDS-PAGE (see Materials and methods). Control samples were obtained from naive oocytes. Note that monomer subunits show an anomalous apparent mass of 62 (predicted mass of 37 kD) and 56 kD after deglycosylation with peptide-*N*-glycosidase F (not depicted); two linked subunits migrate at 97 and 89 kD after peptide-*N*-glycosidase F (not depicted).

Downloaded from jgp.rupress.org on July 6, 2009

Given that residues in P1-TM2 and P2-TM4 are not identical and that P1 and P2 are not equidistant from TM2 and TM4, it is not surprising that the second site mutations most effective for other domain recovery were poorly effective in same domain restoration (i.e., V258D and G134D), that the most potent same domain restoring substitutions (F137D and L257D) were without impact on suppression from the other domain, and that restoring substitutions on same and other domains array differently on helical plots (Fig. 3). These differences argue that second site complementation takes place via a position-specific mechanism.

To confirm that truncation of the channel was not confounding, allowing either for suppression by lysine or second site recovery, full-length $K_{2p}\emptyset$ was studied with S104K or T216K changes (Fig. S1). As with $\Delta K_{2p}\emptyset$, the P1 mutation eliminated ionic currents, and second changes to N133D in TM2 or V258D in TM4 restored flux (Fig. S1, A and B). Likewise, the P2 mutation suppressed activity of full-length channels, and currents were restored by the second changes to L257D in TM4 or G134D in TM2 (Fig. S1, C and D). $\Delta K_{2p}\emptyset$ and full-length channels bearing S104K or T216K and complementary aspartate mutations were generally like WT channels, remaining open at rest and selective for potassium, but often passed smaller outward currents

(Fig. 3). Failure to fully reconstitute WT function was to be expected because pairs of mutations rarely restore native side chain volumes or conduction pathway neutrality (Chatelain et al., 2005) and, thus, the energy landscape experienced by permeating ions.

Subunits linked in tandem recapitulate WT function

If two $K_{2p}\emptyset$ subunits are sufficient to form complete channels, as suggested by studies of proton block of $K_{2p}3$ (Lopes et al., 2001; Yuill et al., 2007) or alkaline activation of $K_{2p}5$ (Niemeyer et al., 2007), it is reasonable to expect that suppression of current by a lysine in P1 might be overcome by an aspartate not only in TM2 of domain I (Fig. 3 A) or TM4 of domain II (Fig. 3 C) but also in TM2 or TM4 of a second subunit contributing to the same ion conduction pore. To test this conjecture, a tandem of two $\Delta K_{2p}\emptyset$ subunits was generated by encoding a five-amino acid linker between the C terminus of one $\Delta K_{2p}\emptyset$ subunit and the N terminus of the next (Fig. 4). For clarity, these $\Delta K_{2p}\emptyset-\Delta K_{2p}\emptyset$ channels are described as bearing four domains (I-II-III-IV).

Currents passed through $\Delta K_{2p}\emptyset-\Delta K_{2p}\emptyset$ channels were slightly larger than WT but otherwise displayed the same macroscopic phenotype, ion selectivity, and rectification attributes as those formed by unlinked $\Delta K_{2p}\emptyset$ subunits (Fig. S2). A single lysine only in P1 (S104K) but not the

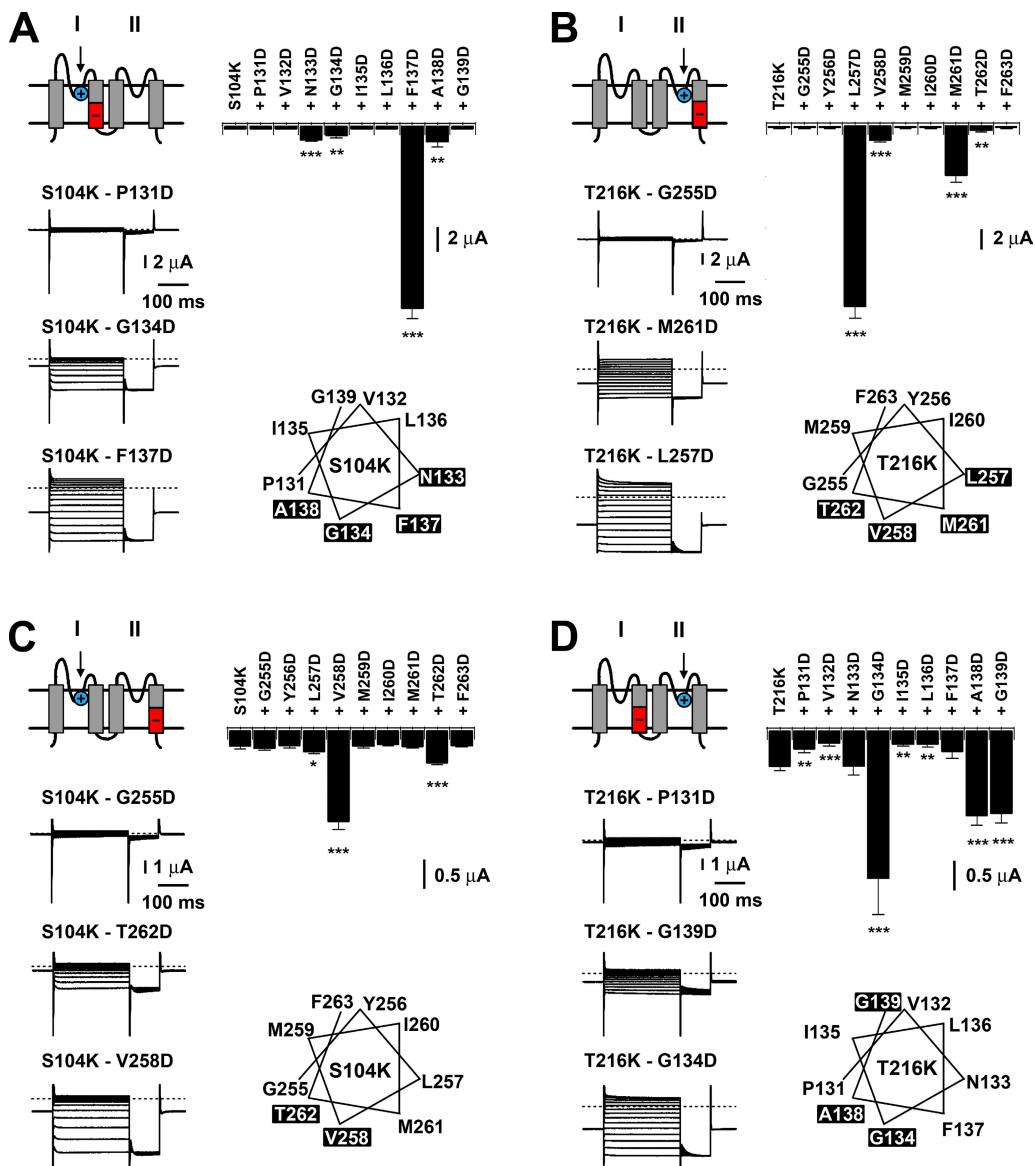


Figure 3. Restoration of $\Delta K_{2p}\emptyset$ channel function by second site changes TM2 or TM4. Currents studied as in Fig. 2 A. Bar graphs show current amplitude \pm SEM at -100 mV. Sample current traces of channels in which second mutations have no impact or show different restoring effectiveness. Topology insets: blue circles denote S104K in P1 or T216K in P2, and red bars indicate the sites in TM2 or TM4 serially altered to aspartate. (A) S104K $\Delta K_{2p}\emptyset$ channels with no other change or second sites altered to aspartate from 131 to 139 in TM2. Statistical differences versus S104K are indicated ($n = 9$). A helical wheel plot indicates four TM2 sites that restore function (133, 134, 137, and 138). (B) T216K $\Delta K_{2p}\emptyset$ channels with no other change or second sites altered to aspartate from 255 to 263 in TM4. Statistical differences versus T216K are indicated ($n = 9$). A helical wheel plot indicates four TM4 sites that restore function (257, 258, 261, and 262). (C) S104K $\Delta K_{2p}\emptyset$ channels with no other change or second sites altered to aspartate from 255 to 263 in TM4. Statistical differences versus S104K are indicated ($n = 10$). A helical wheel plot indicates two TM4 sites that restore function (258 and 262). (D) T216K $\Delta K_{2p}\emptyset$ channels with no other change or second sites altered to aspartate from 131 to 139 in TM2. Statistical differences versus T216K are indicated ($n = 5-10$). A helical wheel plot shows three TM2 sites that restore function (134, 138, and 139). *, $P < 0.05$; **, $P < 0.01$; ***, $P < 0.001$.

three other P loops of $\Delta K_{2p}\emptyset-\Delta K_{2p}\emptyset$ channels reduced currents but did not eliminate flux (Fig. 4 B and Fig. S3, B and C). As expected, based on our studies of monomer subunits (Fig. 2), lysine substitution in both P1 loops of $\Delta K_{2p}\emptyset-\Delta K_{2p}\emptyset$ channels (domains I and III) suppressed current (Fig. 4 B and Fig. S3, B and C). Similarly, lysine in only P2 (T216K) of $\Delta K_{2p}\emptyset-\Delta K_{2p}\emptyset$ diminished current, whereas lysine in both P2 loops (domains

II and IV) silenced the channels (Fig. 4, E–H; and Fig. S3, B and C). Supporting the idea that $\Delta K_{2p}\emptyset-\Delta K_{2p}\emptyset$ channels use all four domains, a single lysine in domain I had the same impact as a lysine in domain III (Fig. S3, B and C). The same was true for a single T216K mutation in domain II or IV (Fig. S3, B and C). Further evidence for this topology was sought through study of electrostatic interactions in channels formed with tandem subunits.

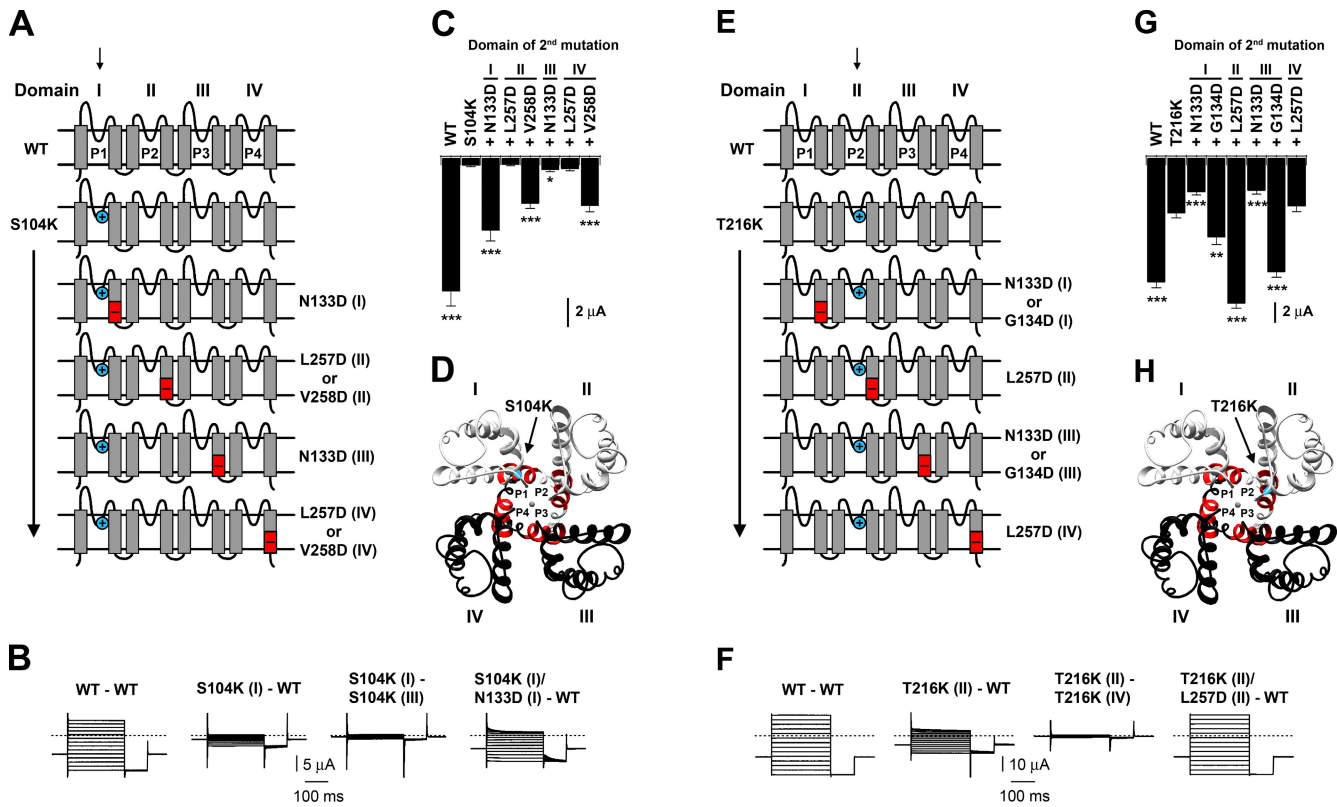


Figure 4. Restoration of $\Delta K_{2p}\emptyset - \Delta K_{2p}\emptyset$ channel currents by second site changes in the same and adjacent domains. Currents suppressed by S104K in domain I of $\Delta K_{2p}\emptyset - \Delta K_{2p}\emptyset$ are restored by second site substitution of aspartate in domains I, II, and IV but not III. Similarly, currents suppressed by T216K in domain II of $\Delta K_{2p}\emptyset - \Delta K_{2p}\emptyset$ are restored by second site substitution in domains I, II, and III but not IV. Currents were studied as in Fig. 2 A. (A) Predicted topology of $\Delta K_{2p}\emptyset - \Delta K_{2p}\emptyset$ with S104K in domain I (blue circles); domains I–IV are indicated, as are TM spans with second site changes (red bars). (B) Currents from $\Delta K_{2p}\emptyset - \Delta K_{2p}\emptyset$ channel variants. To reveal phenotype, oocytes with WT-WT, S104K (I)-WT, and S104K (I)-S104K (III) were incubated for extended periods. (C) Current amplitudes \pm SEM at -100 mV from oocytes expressing S104K (I) $\Delta K_{2p}\emptyset - \Delta K_{2p}\emptyset$ channels with no other change or second sites altered to aspartate as indicated. Statistical differences versus S104K (I) $\Delta K_{2p}\emptyset - \Delta K_{2p}\emptyset$ are indicated ($n = 6$). (D) Top view of a KcsA channel noting positions homologous to S104K in domain I (blue) and TM segments studied in each of four domains (red). (E) Predicted topology of $\Delta K_{2p}\emptyset - \Delta K_{2p}\emptyset$ with T216K in domain II (blue circles); domains I–IV are indicated, as are TM spans with second site changes (red bars). (F) Representative currents from the indicated $\Delta K_{2p}\emptyset - \Delta K_{2p}\emptyset$ channel variants. (G) Current amplitudes \pm SEM at -100 mV from oocytes expressing T216K (II) $\Delta K_{2p}\emptyset - \Delta K_{2p}\emptyset$ channels with no other change or second sites altered to aspartate as indicated ($n = 14$ – 16). (H) Top view of a KcsA channel noting positions homologous to T216K in domain II (blue) and TM segments studied in each of four domains (red). *, $P < 0.05$; **, $P < 0.01$; ***, $P < 0.001$.

Restoration from the same and other subunit

Suppression of current by S104K in P1 of $\Delta K_{2p}\emptyset - \Delta K_{2p}\emptyset$ channels was offset by aspartate substitution in domain I (N133D) or domain II (V258D; Fig. 4 C), as expected from rescue of S104K by N133D in TM2 or V258D in TM4 in monomer subunits (Fig. 3). Although aspartate in domain IV (V258D) of $\Delta K_{2p}\emptyset - \Delta K_{2p}\emptyset$ channels was also restoring (Fig. 4 C), substitution at the homologous position of domain III (N133D) had no significant effect. Thus, lysine in domain I was responsive to complementation by aspartate in the same domain (I), the adjacent domain of the same subunit (II), and the other domain predicted to be adjacent if one tandem subunit folds to create the conduction pathway (IV), but not the domain predicted to be diagonally across the pore (III; Fig. 4 D).

The same pattern of second site complementation was observed with $\Delta K_{2p}\emptyset - \Delta K_{2p}\emptyset$ channels carrying a single

T216K mutation in domain II (Fig. 4, E–H). Thus, function was restored by L257D substitution in domain II and G134D substitutions in the domains predicted to be adjacent to domain II (I and III), whereas L257D in domain IV was ineffective. Indicating that restoring effects were specific to both domain and position, a secondary L257D change in domain II or IV had no impact on suppression by S104K (I) in $\Delta K_{2p}\emptyset - \Delta K_{2p}\emptyset$ channels (Fig. 4 C), and N133D in domain I or III was without restoring effect in T216K (II) $\Delta K_{2p}\emptyset - \Delta K_{2p}\emptyset$ channels (Fig. 4 G).

Charge reversal supports an electrostatic mechanism and a diagonal configuration

If current suppressed by a lysine in P1 (S104K) is restored by an aspartate in TM2 (F137D) or TM4 (V258D) through a direct electrostatic interaction, it is reasonable to expect that reversing the location of the charge

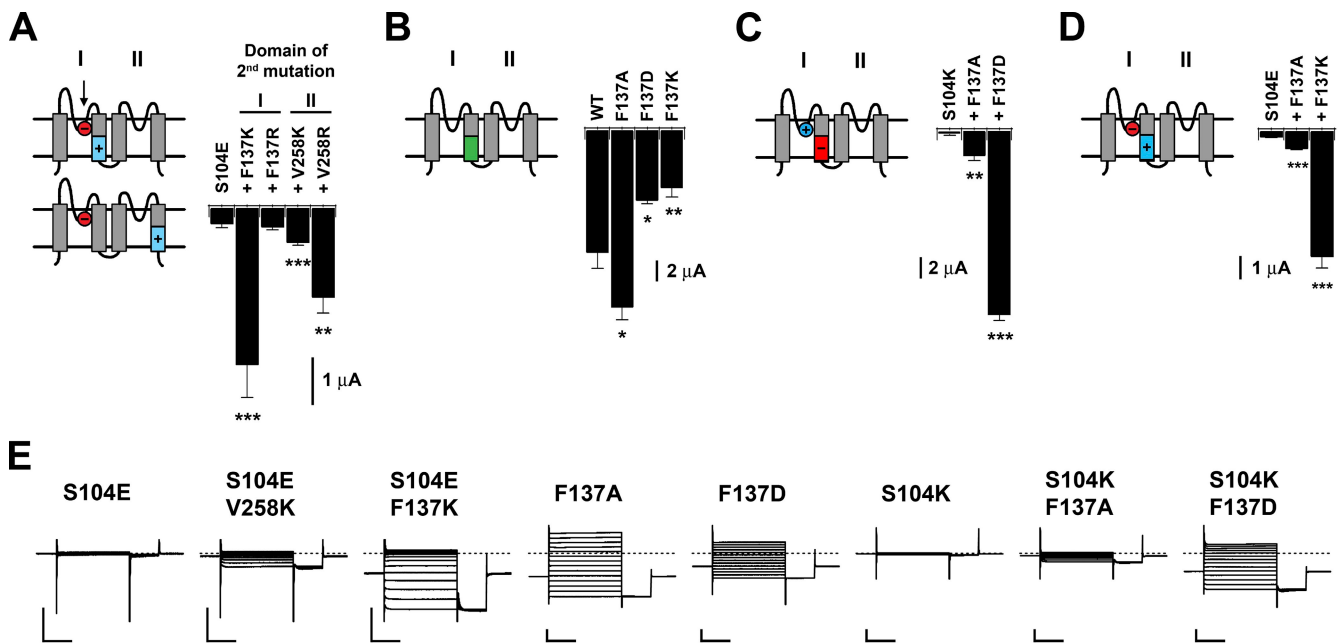


Figure 5. Charge reversal supports an electrostatic mechanism for complementation. Currents were studied as in Fig. 2 A. Bar graphs plot current amplitudes \pm SEM at -100 mV. (A) S104E $\Delta K_{2p}\emptyset$ with no other change, F137 in TM2, or V258 in TM4 altered to lysine (K) or arginine (R). (insets) Glutamate (E) in P1 (red); TM sites studied (blue). Statistical differences versus S104E are indicated ($n = 10$). (B) WT $\Delta K_{2p}\emptyset$ or $\Delta K_{2p}\emptyset$ with single changes at position F137 (green box). Statistical differences versus WT are indicated ($n = 6$ –10). Mutation of F137 increases single-channel activity (i.e., WT, open probability = ~ 0.77 ; F137C, open probability = ~ 0.93) and thereby decreases closed state-dependent Zn^{2+} block (i.e., WT, half-maximal inhibition at equilibrium (K_i) = 5 μ M; F137A, K, and D, $K_i \gg 1$ mM) by reported methods (Zilberberg et al., 2001). (C) S104K $\Delta K_{2p}\emptyset$ channels with no other change or second site changes at F137. (inset) S104K in P1 (blue); TM2 site studied (red). Statistical differences versus S104K are indicated ($n = 4$ –10). (D) S104E $\Delta K_{2p}\emptyset$ channels with no other change or second site changes at F137. (inset) S104E in P1 (red); TM2 site studied (blue). Statistical differences versus S104E are indicated ($n = 6$ –8). (E) Sample current traces for the indicated $\Delta K_{2p}\emptyset$ channels with one or two mutations. Bars, 5 μ A and 100 ms. *, $P < 0.05$; **, $P < 0.01$; ***, $P < 0.001$.

substitutions should replicate the findings. Indeed, mutation of S104 to glutamate (S104E) eliminated ion flux, and second site substitution of lysine in TM2 (F137K) or TM4 (V258K) restored currents (Fig. 5, A and E). These findings argue against an allosteric mechanism wherein the local impact of S104K is nonspecifically overcome by an unrelated countereffect of aspartate in TM2 or TM4; oppositely charged K and E substitutions at 104 would be expected to have different local effects, as would D and K at positions 137 or 258. The change S104E was used because aspartate at 104 did not suppress current effectively (unpublished data).

We were explicitly concerned about ruling out increased channel activity as a nonspecific basis for current restoration because we found changes at position 137 to influence single-channel open probability. For example, F137A channel currents are larger than those of WT channels (Fig. 5 B). Arguing against this type of indirect mechanism, channels with the single mutation F137D or F137K passed currents of lower magnitude than WT channels (Fig. 5 B), and F137A did not restore current to S104K like F137D (Fig. 5 C) nor complement S104E like F137K (Fig. 5 D).

The findings with tandem subunits argue that $\Delta K_{2p}\emptyset$ channels are built from two subunits arranged in a circular fashion (like voltage-gated sodium channel subunits

that have four linked homologous domains) with identical P loops positioned diagonally across the ion conduction pathway from each other because two S104 residues and two T216 residues contribute to pore formation whether they are supplied by two monomer subunits or one tandem (Fig. 4, Fig. S2, and Fig. S3). In addition, current can be restored by charge–charge complementation between residues in the same domain, adjacent domains of the same subunit, or adjacent domains of subunits linked in tandem. A model was pursued.

Pore exposure inferred by effects of aspartate substitution
To model $\Delta K_{2p}\emptyset$ by homology, it was first necessary to assign an alignment register for its TM segments and those in channels with determined crystal structures (Baker and Sali, 2001). To deduce pore exposure, aspartate was introduced into TM2 and TM4 sites in the absence of other changes. An added charge is often tolerated at TM positions that face the aqueous pore, whereas they are frequently disruptive at sites of protein–protein or protein–lipid interaction (Collins et al., 1997; Chen and Goldstein, 2007). Consistent with pore exposure, macroscopic recordings reveal aspartate to be tolerated at five of nine positions in TM2 (N133, G134, F137, A138, and G139) and four of nine positions

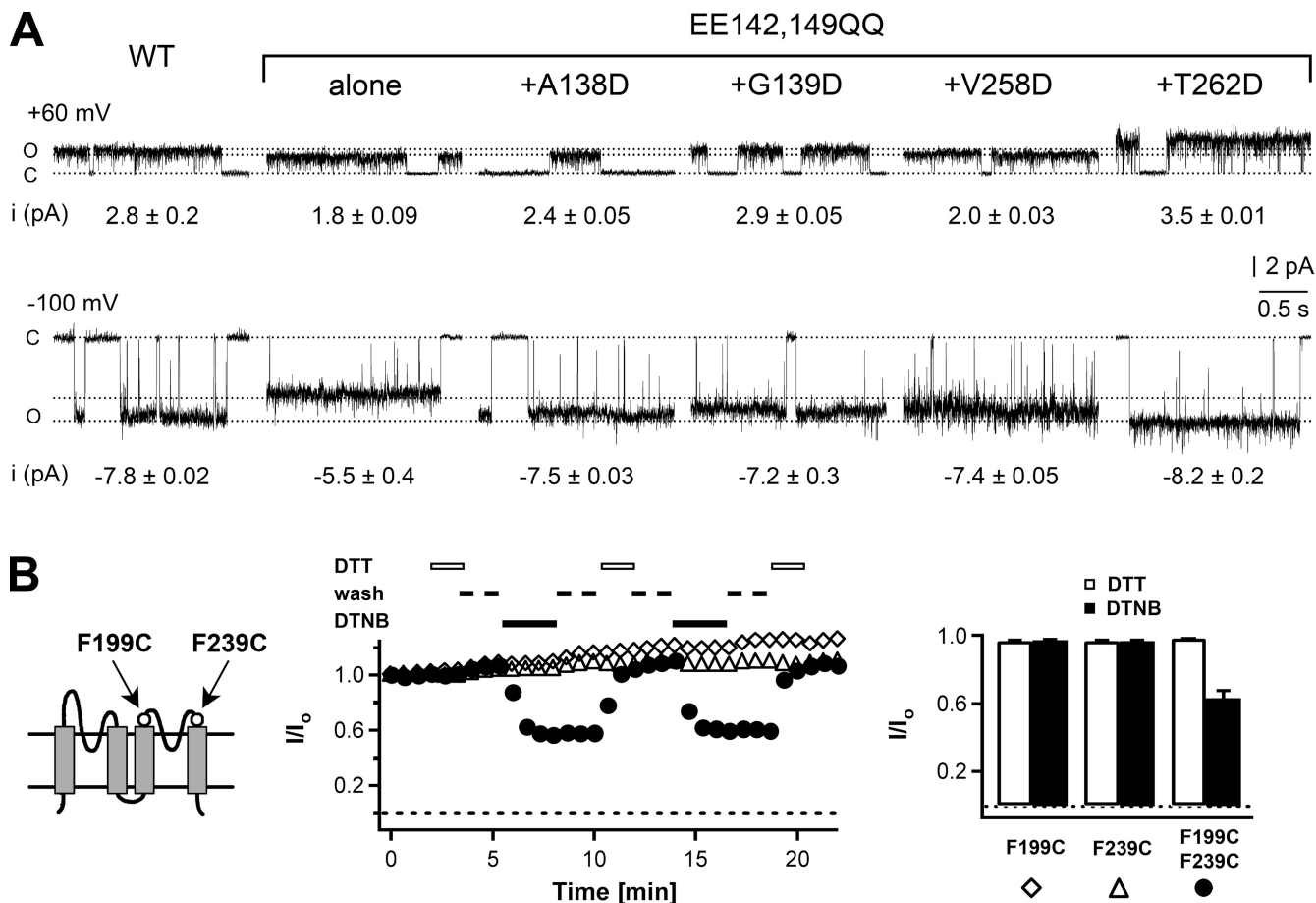


Figure 6. Pore exposure and residue proximity inferred by site effects on single-channel current or disulfide bond formation. (A) Single WT $\Delta K_{2p}\emptyset$ channels or EE142,149QQ $\Delta K_{2p}\emptyset$ channels with no other change or the indicated third mutation studied at 60 and -100 mV in on-cell patches with 140-mM KCl solution in the bath and pipette (see Materials and methods). Unitary currents (i) were determined from 2 to 8.5 min of recording from two to six patches sampled at 20 kHz, filtered at 5 kHz with one to nine channels per patch (median = 2), and noted \pm SEM. Exemplar currents were filtered at 500 Hz. Open (O) and closed (C) levels are indicated. (B, left) Predicted topology of $\Delta K_{2p}\emptyset$ indicating the location of F199 and F239. (middle) Whole cell currents studied at 30 mV. The channels studied had the native external cysteine in the first external loop altered to serine (C73S). Application of 0.5 mM DTNB reduces C73S F199C F239C $\Delta K_{2p}\emptyset$ current (black circles), and 5 mM DTT reverses the effect. Current of $\Delta K_{2p}\emptyset$ C73S F199C (open diamonds) or C73S F239C $\Delta K_{2p}\emptyset$ (open triangles) is not affected by exposure to DTT or DTNB. Plot is normalized current for single cells; every 20th data point. (right) Current \pm SEM at 30 mV after application of 5 mM DTT (open bars) or 0.5 mM DTNB (closed bars) normalized to the amplitude of the same cell without treatment for $\Delta K_{2p}\emptyset$ channels with the following changes: C73S and F199C; C73S and F239C; C73S and F199C and F239C ($n = 2-4$ cells).

in TM4 (L257, V258, M261, and T262; Fig. S4, A and B). Disruption of channel function by aspartate at V132, I135, and L136 in TM2 and G255, Y256, M259, I260, and F263 in TM4 suggests these sites face away from the pore, as does the failure of S104K or T216K to restore function to these variants.

Single-channel interrogation supported pore exposure of A138, G139, V258, and T262. Two negatively charged residues per subunit naturally near the cytoplasmic entrance of a mammalian calcium-activated potassium channel (mBK) or introduced at homologous sites in KcsA increase single-channel conductance apparently by raising the local potassium concentration (Brelidze et al., 2003; Nimigean et al., 2003; Carvacho et al., 2008). $\Delta K_{2p}\emptyset$ residues E142 and E149 lie in similar

positions of TM2 (Fig. S4 C), and, as predicted, neutralization of the sites by mutation (EE142,149QQ) lowered single-channel current relative to WT by 36% at 60 mV (Fig. 6 A). Aspartate added into EE142,149QQ $\Delta K_{2p}\emptyset$ channels at A138, G139, V258, or T262 increased unitary current consistent with exposure to the aqueous pore. The sequence alignment was based on these observations (Fig. S5).

A model for $K_{2p}\emptyset$ adopts bilateral symmetry

A ribbon diagram of the refined three-dimensional model of $K_{2p}\emptyset$ is shaped like a parallelogram when viewed en face from the external surface (Fig. 7 A) or cytoplasm (Fig. 7 B). The selectivity filter is fourfold symmetric as in potassium channels with four subunits

(Fig. 7, A–D). The steps taken to create the three-dimensional model included sequence alignment with crystallized potassium channels, relaxation of all residues using MD, energy minimization, and refinement based on comparison of effects of pairs of mutations with model-based continuum electrostatics calculations that determine the free energy barrier (ΔG) that a potassium ion must overcome when moving from the intracellular solution to the selectivity filter. Thus, ΔG was much higher for S104K and T216K channels than for WT and was reduced by introduced countercharges that restored function but not by those that did not complement (Fig. 7 E). All but 3 of 57 channel variants met expectations of calculations based on the refined model as demonstrated by evaluation of the maximal difference between WT and mutant channels ($\Delta\Delta G$), a measure of the dominant free energy barrier for ion conduction relative to the WT (Fig. 7 F, Fig. S6, and Table I); the outliers (F137R, G139D, and M261D) will be considered further in the Discussion.

As detailed in the Materials and methods section, the primary structural template was chosen to be the crystal structure of $K_v1.2$ in the open state (Long et al., 2005) because pairwise electrostatic interactions that we determined to permit ion conduction required an active conformation. Sequence alignment also included four other crystallized potassium channels: K_vAP , $K_{cs}A$, $K_{ir}Bac1.1$, and $MthK$ (Doyle et al., 1998; Jiang et al., 2002, 2003; Kuo et al., 2003). Alignment is key to the resultant model (Baker and Sali, 2001) and required adjustment (see Materials and methods) based on positions in TM2 and TM4 of $K_{2p}\emptyset$ inferred to be pore exposed in functional experiments (Fig. 6, Fig. S4, and Fig. S5). Neither symmetry nor location of individual residues was otherwise imposed. $K_{2p}\emptyset$ domains I and II were arranged in a clockwise fashion viewed from the outside because the TM2–TM3 linker is too short for unrestrained folding in a counter-clockwise orientation. Helical distortions at P131 in TM2 (a residue conserved in most K_{2p} channels) and P183 and P192 in TM3 (the latter is in several K_{2p} channels) were allowed. The model was refined by MD and energy minimization with potassium ions in filter positions S1 and S3 and a water molecule in S2 and by comparing the results of second site compensation and continuum electrostatic calculations based on the finite difference Poisson-Boltzmann equation (Honig and Nicholls, 1995; Roux and MacKinnon, 1999; Roux et al., 2000).

Disulfide bond formation supports proximity of residues in the model

In the $K_{2p}\emptyset$ model, the C_β atoms of E28 and T115 are separated by 5.0 and 5.1 Å in the two subunits, with their side chains oriented toward each other (Fig. 7 G). Consistent with proper alignment of the TM segments and the resultant model, a disulfide bond was previously observed to form spontaneously when these sites were both mutated to cysteine, holding the channels in

the closed state until reductant was applied (Zilberberg et al., 2001).

Similarly, the C_β atoms of F199 and F239 are separated by 6.7 and 6.9 Å in the two subunits of the model, with their side chains in proximity (Fig. 7 H). In further support of the model, channels with both F199C and F239C showed a decrease in current on exposure to the oxidizing agent DTNB, current inhibition was steady despite DTNB washout until exposure to the reductant DTT, and channels with only F199C or F239C were insensitive to DTNB and DTT (Fig. 6 B). Residue E200 (homologous to E28) was not studied because E200C channels were nonfunctional (Zilberberg et al., 2001).

Electrostatic compensation correlates with modeled distance between residues

Chatelain et al. (2005) showed that aspartates at three positions modeled to be pore exposed on successive helical turns restored current with increasing effectiveness according to their proximity to the lysine in the pore. Complementation effectiveness was found to be similarly distance dependent in $\Delta K_{2p}\emptyset$ (Table I and Fig. 7 I). Thus, $\Delta K_{2p}\emptyset$ channels silenced by T216K were rescued by aspartate with less potency as the distance between the substituted residues increased. Similarly, $\Delta K_{2p}\emptyset$ – $\Delta K_{2p}\emptyset$ channels silenced by T216K in domain II showed less restoration with increasing distance: L257D (II), 7 Å > G134D (III), 12 Å > G134D (I), 13 Å (Fig. S6 A). So, too, complementation of monomer and tandem channels silenced by S104K and monomer S104E channels followed the same pattern (Fig. S6, C, E, and G) with the exception of F137D, a change that was more potent than expected, most likely as a result of nonelectrostatic effects of changes at this position on open probability (Fig. 5, B–D).

Electrostatic compensation occurs when the unfavorable effect of a charged amino acid (i) on permeating ions is offset by the addition of a second countercharge (j). Because this occurs most effectively when the two charged residues are colocated, compensation effectiveness should change with the distance between residues i and j in a predictable manner (Fig. S7). Thus, electrostatic compensation can be exploited to deduce structural constraints on a channel. The distance dependence of compensation in this case does not reflect through-space electrostatic interaction of the charged residues i and j but their opposite effects on permeating ions (a third charge). In contrast, direct electrostatic interaction between charged residues i and j can be probed, for example, through mutant cycle analysis (Hidalgo and MacKinnon, 1995; Ranganathan et al., 1996; Tiwari-Woodruff et al., 1997, 2000).

Reliability of the model

Fourfold symmetry is observed in potassium channels of known structure, all of which are formed by four identical subunits (Doyle et al., 1998; Jiang et al., 2002,

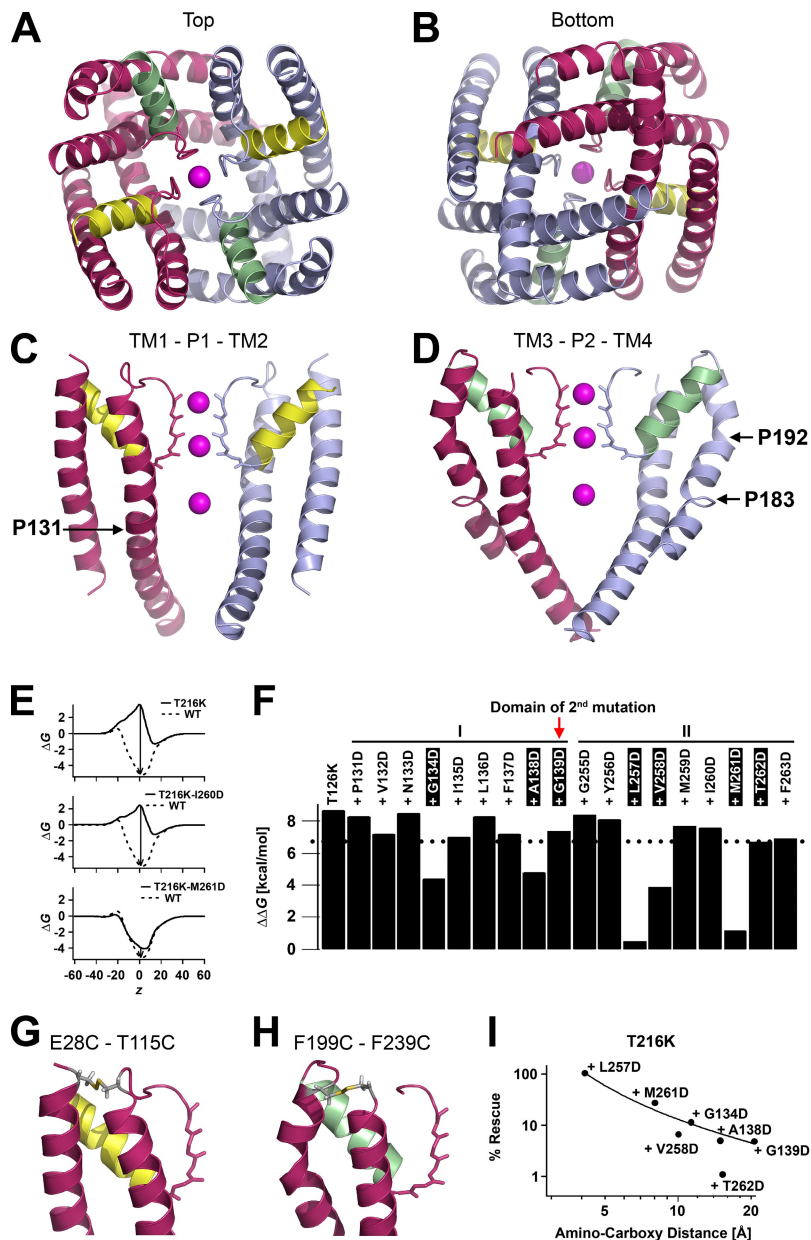


Figure 7. A homology model for $\Delta K_{2p}\emptyset$ channels shows bilateral symmetry with a fourfold symmetric selectivity filter. Model building, refinement, and electrostatic calculations are described in Materials and methods. One subunit is colored in magenta, and the second is colored in blue. The P1 pore helices are in yellow, and P2 pore helices are in green. A file with the main chain coordinates is included in the supplemental material (available at <http://www.jgp.org/cgi/content/full/jgp.200910235/DC1>). (A) The model of $K_{2p}\emptyset$ from the extracellular side reveals overall symmetry like a parallelogram. The model includes residues 1–276 without the TM1-P1 loop (residues 30–91), TM2–TM3 linker (residues 153–173), and TM2-P2 loop (residues 225–238). (B) Model of $K_{2p}\emptyset$ viewed from the cytoplasm. (C) Side view of domain I of both subunits. Pro131 in TM2 is indicated. (D) Side view of domain II of both subunits. Proline residues in TM3 are indicated. (E) Illustration of electrostatic calculations to ascertain the effect of charged mutations on ion permeation (static field contribution). (top) $\Delta\Delta G$ for T216K $\Delta K_{2p}\emptyset$: ΔG for the T216K channel (solid line) and ΔG for the WT channel (dashed line) are shown along the pore axis. The membrane bilayer spans $z = -12.5$ to $z = 12.5$; $\Delta G = \max[|\Delta G_{T216K} - \Delta G_{WT}|]$. This definition of $\Delta\Delta G$ provides a measure of the dominant free energy barrier for ion conduction relative to the WT channel. The arrow indicates where $\Delta\Delta G$ is evaluated. (middle and bottom) Same calculations for T216K-I260D (no rescue) and T216K-M261D (rescue), respectively. (F) Electrostatic $\Delta\Delta G$ (static field contribution) for T216K $\Delta K_{2p}\emptyset$ channels with second site alterations to aspartate (131–139 in TM2 or 255–263 in TM4). Black shading indicates 7 of 18 mutations that restore current. The highest $\Delta\Delta G$ where complementation was observed is marked with a dotted line. The red arrow notes G139D. (G) Section of C showing a disulfide bridge between residues E28C and T115C; the S–S distance in the two subunits (C_β – C_β) are 5.0 and 5.1 Å. (H) Section of D showing a disulfide bridge between residues F199C and F239C; the S–S distance in the two subunits (C_β – C_β) are 6.7 and 6.9 Å. (I) Effectiveness of complementation as a function of distance for T216K $\Delta K_{2p}\emptyset$ channels. Rescue percentage was determined at -100 mV as $(I_{\text{Mut}} - I_{T216K}) / (I_{\text{WT}} - I_{T216K})$. Distances were measured as in Table I. Data were fit to $f(x) = (e^{b/x} - 1)$.

2003; Kuo et al., 2003; Long et al., 2005). The model of $K_{2p}\emptyset$ shows bilateral symmetry. To a point, this is expected for a complex of two subunits, each with two nonidentical domains (Fig. S4). To explicitly assess enforced fourfold symmetry, a new model was created by maintaining the backbone structure of Kv1.2 and allowing only $K_{2p}\emptyset$ side chains to relax (rather than permitting simultaneous relaxation of backbone and side chain atoms). The resultant fourfold model yields electrostatic $\Delta\Delta G$ values that deviate from experimental observation for 11/57 channel mutants (Fig. S8). Comparison of the fourfold and bilateral models on the basis of RMSD of main chain atoms suggests the former must be altered

by ~ 2.9 Å to achieve good agreement of model-based calculations and experimental data.

DISCUSSION

K_{2p} channels: two subunits, bilateral symmetry, and one pore

Given that potassium channels formed by subunits with one P loop are tetramers (MacKinnon, 1991; Doyle et al., 1998), the presence of two P loops in a single subunit suggested K_{2p} channels would use four P loops from two subunits (Ketchum et al., 1995; Fink et al.,

1996; Goldstein et al., 1996). To confirm this expectation and gain insight into the structure of $K_{2p}\emptyset$ channels, we examined the relationship of the two P loops and their following TM segments in $K_{2p}\emptyset$ through a study of charge–charge interactions of substituted amino acids. A charged residue in P1 (S104K or S104E) or P2 (T216K) suppressed channel function without loss of surface expression (Fig. 2). Channel activity was restored by a second mutation of opposite charge in specific TM2 or TM4 positions (Fig. 3). Experiments with two subunits linked in tandem showed two P1 loops and two P2 loops in the channel pore, similar roles for P1 and P2 in channel function, and formation of a single conduction pathway where P1 interacts directly with domains I, II, and IV but not domain III diagonally across the pore and P2 interacts with domains I, II, and III but not IV (Fig. 4). A three-dimensional model of the $K_{2p}\emptyset$ channel with two subunits, shaped like a parallelogram when viewed from the cytosol or external surface, and with a fourfold symmetric selectivity filter is adequate to explain these findings and cross-linking of two pairs of introduced cysteines (Fig. 7).

Evidence for electrostatic compensation by pairs of introduced charges

The hypothesis that complementation is caused by electrostatic compensation by charged amino acids is supported by at least six lines of evidence (Figs. 3–5 and 7). (1) Single mutations that reduce current amplitudes below WT level when introduced on their own restore activity to channels silenced by a countercharge. (2) Restoration is observed on pairwise reversal of the charges in P1 and TM2 (S104K with F137D and S104E with F137K) or P1 and TM4 (S104K with V258D and S104E with V258R), arguing against counteracting but unrelated effects of primary and secondary mutations at separate locations. (3) Second site mutations that increase open probability are not sufficient to complement; F137D cannot rescue T216K channels, nor can F137A restore operation to S104K and S104E channels as F137D and F137K do, respectively. (4) The same substitution at the same position in homologous domains of $\Delta K_{2p}\emptyset$ – $\Delta K_{2p}\emptyset$ tandem channels complements only a specific primary mutation; for example, N133D in domain I restores current to a channel with lysine in the same domain (S104K in domain I), whereas N133D in domain III is not effective. (5) Observed second site complementation correlates with model-based calculations of the energy barriers for potassium ion movement from the cytosol to the selectivity filter. (6) The effectiveness of complementation depends on the modeled distance between interacting residues.

Local electrostatic environment and electrostatic compensation

Four specific conditions must be fulfilled to reverse inhibition by lysine in the pore via electrostatic compensation: (1) tolerance for the second site mutation to aspartate,

TABLE I

Distances between pairs of introduced residues and electrostatic ΔG values based on the $K_{2p}\emptyset$ model

Mutation	Distance to S104 or T216 $C_\beta-C_\beta$ ($\epsilon N-C$)	$\Delta\Delta G$ versus WT kcal/mol
	Å	
Second site mutations that complement		
<i>Monomer subunits</i>		
S104K alone		7.9
+N133D	7.6 (3)	0.3
+G134D	11.1 (10)	5.2
+F137D	12.0 (8)	1.3
+A138D	16.2 (15)	5.9
+V258D	12.9 (7)	0.8
+T262D	18.7 (16)	6.5
T216K alone		8.7
+L257D	8.8 (4)	0.5
+V258D	13.1 (10)	3.9
+M261D	12.4 (8)	1.2
+T262D	17.5 (15)	6.7
+G134D	14.6 (11)	4.4
+A138D	19.0 (15)	4.8
+G139D	22.8 (21)	7.4
S104E alone		6.9
+F137K	12.0 (4)	1.1
+V258K	12.9 (7)	1.6
+V258R	12.9 (4)	1.8
<i>Tandem subunits</i>		
S104K (I) alone		4.1
+N133D (I)	7.6 (3)	0.5
+V258D (II)	12.9 (10)	2.3
+V258D (IV)	20.0 (15)	3.5
T216K (II) alone		5.1
+G134D (I)	15.8 (13)	3.1
+L257D (II)	8.8 (7)	0.5
+G134D (III)	14.6 (12)	3.1
Second site mutations that do not complement		
<i>Monomer subunits</i>		
S104K alone		7.9
+P131D	13.3 (13)	8.2
+V132D	11.6 (13)	8.4
+I135D ^a	15.2 (16)	7.1
+L136D	13.4 (15)	7.9
+G139D ^a	18.2 (19)	7.2
+G255D	13.1 (15)	7.6
+Y256D	16.2 (17)	8.3
+L257D	12.8 (12)	7.9
+M259D	17.8 (17)	7.8
+I260D	19.2 (18)	7.8
+M261D ^a	15.9 (12)	3.9
+F263D ^a	22.4 (21)	7.3
T216K alone		8.7
+G255D	14.2 (17)	8.4
+Y256D	13.1 (15)	8.1
+M259D	16.0 (17)	7.7
+I260D	13.9 (14)	7.6
+F263D ^a	18.3 (19)	6.9

TABLE I (Continued)

Mutation	Distance to S104 or T216 C _β -C _β (ε N-C)	$\Delta\Delta G$ versus WT
+P131D	12.8 (12)	8.3
+V132D	15.5 (14)	7.2
+N133D	14.8 (11)	8.5
+I135D ^a	18.2 (16)	7.0
+L136D	20.3 (18)	8.3
+F137D	15.8 (13)	7.2
S104E alone		6.9
+F137R ^a	12.0 (4)	1.2
<i>Tandem subunits</i>		
S104K (I) alone		4.1
+L257D (II)	12.8 (13)	3.6
+N133D (III)	20.1 (15)	5.0
+L257D (IV)	18.4 (19)	4.2
T216K (II) alone		5.1
+N133D (I)	15.8 (13)	4.1
+N133D (III)	14.8 (11)	4.7
+L257D (IV)	20.8 (16)	4.0

Values for monomer subunits and those linked in tandem were determined (see Materials and methods). The presented distances are between C_β-C_β in the WT model and the closest approach of the ε -amino of suppressive lysine and carboxylate carbon of restoring aspartate in mutant models (ε N-C). $\Delta\Delta G$ values are the difference between WT and mutant for the electrostatic free energy barrier that a potassium ion has to overcome traveling from the intracellular solution to the selectivity filter. pK_a calculations predict that all second site changes that complement are charged.

^aSeven second site mutants are predicted to be charged but do not complement; five of these do not appreciably lower $\Delta\Delta G$; F137R is predicted to rescue, but might be too close to S104E, resulting in steric hindrance, because two large residues cannot be accommodated in the available space. Discrepancy between experimental and computational results on rescue of S104K by M261D might indicate inaccuracy of the model.

(2) proximity of the restoring aspartate and suppressive lysine, (3) a local environment that permits deprotonation of the aspartate, and (4) no shielding of the charge from long-range electrostatic interactions. The third and fourth conditions act in opposition. A hydrophobic environment, which is required for the long-range electrostatic interactions permitting current restoration, can prevent deprotonation of aspartate, whereas aspartate surrounded by water facilitates deprotonation, but its charge can only be sensed over short distances (Carvacho et al., 2008). How the pK_a of an amino acid side chain is influenced by local electrostatics has been studied (Niemeyer et al., 2007; Li et al., 2008). For example, aspartate in the nicotinic acetylcholine receptor facing membrane lipid tends to be neutral, whereas access to the aqueous milieu of the ion conduction pathway favors the deprotonated negatively charged form (Cymes et al., 2005). To assess the state of each aspartate introduced into K_{2P}O, a new model was generated for each mutant, and the pK_a of the substituted aspartate was evaluated using continuum electrostatic calculations to assess the reversible work required to protonate the side chain (see Materials and methods).

Lysine or glutamate introduced at S104 or T216 silence K_{2P}O and were calculated to be charged. All residue substitutions in the TM segments that led to current restoration were also calculated to be charged (Table I). Conversely, 23 of the 30 substitutions that did not complement were predicted to be neutral and, thus, unable to compensate for the suppressive pore charge (Table I). Of note, a direct correlation between the effectiveness of an aspartate in current restoration and its impact on unitary conductance was neither expected nor observed. Thus, T262D increased unitary conductance more than V258D in the absence of a disruptive lysine and after removal of two native negative residues in each subunit (Fig. 6 A), whereas V258D compensated for S104K in an otherwise WT channel more effectively than T262D (Fig. 3 C). Rescue of permeation is rationalized by electrostatic effects that offset each other, whereas unitary conductance is more sensitive to the locations of the various local free energy barriers and wells.

Although electrostatic compensation can be exploited to place spatial constraints on channel structure because the two oppositely charged residues act on permeating ions in a distance-dependent manner, physical proximity of the added charges also influences the pK_a of the introduced aspartate. For example, F137D is closer (13 Å) than A138D (15 Å) to T216K in the model but does not complement (as it does S104K) apparently because it is neutral when the lysine is located in the other channel domain. Similarly, N133D and L257D are charged and complement S104K and T216K, respectively, in tandem dimer channels only when they are positioned in the same channel domain; they are neutral and ineffective when located in the equivalent domain across the pore. Five second site substitutions that fail to complement were judged to be charged but did not appreciably lower $\Delta\Delta G$ because they are too distant (Table I). Two second site changes that fail to complement (and a third that does) do not match predictions based on the three-dimensional model. These are considered next.

Limitations of the study

Although 21 of 22 channels that show second site complementation manifest attributes consistent with the model and an electrostatic mechanism for current restoration, recovery of T216K channel function by G139D mutation does not (Table I). The outlier status of G139D is suggested first by the observation that the residue plots to the opposite face of a helical wheel from other residues that complement T216K in monomer channels (Fig. 3 D). Moreover, the model that accommodates the 21 other charge-charge pairs and two pairs of substituted cysteines that cross-link suggests G139D has limited access to the conduction pore because it resides in a crevice near charged residues in TM1, TM2, and TM4 (Fig. S9), where it may complement by an indirect mechanism.

Calculations suggest that M261D and F137R should complement S104K and S104E, respectively, but they do not (Table I). This could accrue from a failure to identify pairwise interactions that create a stable, closed conformation, as observed for interactions between P-loop residues and the inner TM helix of $K_{IR}3.4$ (Rosenhouse-Dantsker and Logothetis, 2007). Indeed, a bias toward the closed state might explain the lower than expected current amplitude of S104K restored by N133D. Reciprocally, F137D is thought to increase open probability to yield a more robust than expected complementation of S104K.

Alternatively, dashed expectations may result from inaccuracies in the three-dimensional model or approximations in continuum electrostatic calculations. The template and alignment used for creating a model strongly influence the resultant structure (Baker and Sali, 2001). Thus, models for the open state of KcsA based on MthK and K_vAP produce different outcomes (Jogini and Roux, 2005). It should be emphasized that a solely computation-based alignment was insufficient in the present case and that experimental data on backbone structure was absolutely required (see Materials and methods). Electrostatic free energy calculations also bear uncertainty, first because they are based on static protein structures and do not take into account changes in side chain conformation during function. Second, Poisson-Boltzmann calculations to determine ΔpK_a require dielectric constants to be assigned to protein, solvent, and membrane. Although values for bulk solvent and membrane are commonly accepted to be 80 and 2, respectively (White and Wiener, 1996), the choice for the protein is much more uncertain. The dielectric constant of a macromolecule is a surrogate for complex effects, including electronic polarization and atomic vibrations and fluctuations (Gilson and Honig, 1986; King et al., 1991; Schutz and Warshel, 2001). Thus, model-based calculations may fail to discern subtle steric interferences by the large side chains of substituted residues in F137R/S104E channels, although the overall model is valid. The restoration patterns manifest in helical wheel plots (Fig. 3) and parsimony of model and observation in 54/57 cases argue against other misattributions.

$K_{2P}\emptyset$ model and known potassium channel structures

Although all crystallized potassium channels are four-fold symmetric throughout, the ribbon diagram of $K_{2P}\emptyset$ reveals a parallelogram. A cross section through a space-filling model of $K_{2P}\emptyset \sim 4$ Å below the selectivity filter exposes a parallelogram with diagonal distances of ~ 21 Å between the two I130 residues and ~ 15 Å between the L257 residues (Fig. S10). The shape of the cross section changes along the pore axis but remains bilaterally symmetric within the cavity. This was, perhaps, to be expected because only 9% of residues in the two domains of $K_{2P}\emptyset$ are identical. The major differences between the two domains originate from the disposition of three prolines: P131, which is highly conserved in the canonical

TM2 glycine-isoleucine-proline (GIP) motif of K_{2P} channels (Fig. S5), has a strong influence on the curvature of the inner helix (Fig. 7 C); moderately conserved P192 and unique P183 in TM3 bend the outer helix (Fig. 7 D).

The $K_{2P}\emptyset$ model is fourfold symmetric at the selectivity filter. Calculations of the static field contribution to the electrostatic free energy barrier indicate that despite differences in sequence, stabilization of the cavity ion in $K_{2P}\emptyset$ by its pore helices ($\Delta G = -5.6$ kcal/mol) is not vastly different from K_vAP ($\Delta G = -7.3$ kcal/mol), $K_v1.2$ ($\Delta G = -7.6$ kcal/mol), or KcsA ($\Delta G = -8.2$ kcal/mol; Jogini and Roux, 2005). Furthermore, potassium ions are held fourfold symmetrically between eight carbonyl oxygens in the $K_{2P}\emptyset$ model (Fig. 7, C and D) as in the crystal structure of KcsA (Zhou et al., 2001). Also, four threonines stabilize the cavity ion with its water molecules at the bottom of the KcsA selectivity filter (Zhou et al., 2001), and these are conserved in both P loops of all K_{2P} channels (ST¹⁰⁵VGYGN in P1 and TT²¹⁷IGFGD in P2 of $K_{2P}\emptyset$). Indeed, potassium channels formed of nonidentical subunits are described in the K_v (Castellano et al., 1997), K_{IR} (Casamassima et al., 2003), and K_{2P} families (Czirjak and Enyedi, 2002). As their constituent subunits differ, such channels are not fourfold identical, and yet, like $K_{2P}\emptyset$ channels, they are effective potassium-selective portals.

A glycine conserved in most potassium channels and called the “gating hinge” (Jiang et al., 2002) is found in TM2 of K_{2P} channels (within the GIP motif) and is near the bottom of the selectivity filter in the $K_{2P}\emptyset$ model (Fig. S5). A glycine in TM4 located two positions further C terminal in the alignment is also faithfully preserved in K_{2P} channels. This location does not appear to reflect an error but rather asymmetry of the domains because both glycines are present in MthK and a serine is in the classical hinge position in $\sim 3\%$ of potassium channels (Rosenhouse-Dantsker and Logothetis, 2007).

K_{2P} model and operation

Closing of $K_{2P}\emptyset$ was argued to resemble C-type inactivation in Shaker channels based on control of the gating transition in both cases by external pore blockade, external permeant ion, conserved amino acids of impact, shared positions of influence, and formation of disulfide bonds between homologous sites in a state-dependent manner: E28C and T115C in the closed state of $K_{2P}\emptyset$ (Zilberberg et al., 2001). Formation of a disulfide bridge in this study between $K_{2P}\emptyset$ residues F199C and F239C (Fig. 6 B) suggests that comparable gating movements take place in both channel domains. In KcsA, C-type inactivation gating has been shown to depend on the interaction of E71 at the bottom of the pore helix and D80, the last amino acid of the selectivity filter consensus sequence (Cordero-Morales et al., 2006). The three-dimensional model of $K_{2P}\emptyset$ appears to allow a similar interaction in P1 between T101 and N110 in the presence of a water molecule behind the

filter, as reported for KcsA E71S (Cordero-Morales et al., 2007). Indeed, calculations suggested that coordination of a water molecule by the equivalent residues of K_{2P}3 is key to stabilization of the selectivity filter (Stansfeld et al., 2008).

Other K_{2P} channels are expected to have a structural arrangement similar to that described here for K_{2P}Ø. Thus, a role for both P1 and P2 in K_{2P} channel function is inferred from the influence of both domains on ion permeation through K_{2P}3 (Lopes et al., 2001; Yuill et al., 2007) and K_{2P}5 (Niemeyer et al., 2007). Similarly, both P1 and P2 of the eight-TM TOK1 channel from *Saccharomyces cerevisiae* yield changes in potassium conductance (Ketchum et al., 1995; Roller et al., 2005). The K_{2P} model will improve with studies that refine register of the TM segments or directly assess structure.

We wish to thank N. Zilberberg for serving as a generous early mentor to A. Kollewe and thank L. Cuello, N. Goldstein, D. Levy, and A. Lewis for sharing insights during the course of these studies.

This work was supported by the National Institutes of Health (grant RO1GM62342 to B. Roux and grant RO1HL61657 to S. A.N. Goldstein).

Christopher Miller served as editor.

Submitted: 31 March 2009

Accepted: 09 June 2009

REFERENCES

- Antosiewicz, J., J.A. McCammon, and M.K. Gilson. 1996. The determinants of pKas in proteins. *Biochemistry*. 35:7819–7833.
- Baker, D., and A. Sali. 2001. Protein structure prediction and structural genomics. *Science*. 294:93–96.
- Bashford, D., and M. Karplus. 1990. pKa's of ionizable groups in proteins: atomic detail from a continuum electrostatic model. *Biochemistry*. 29:10219–10225.
- Bautista, D.M., Y.M. Sigal, A.D. Milstein, J.L. Garrison, J.A. Zorn, P.R. Tsuruda, R.A. Nicoll, and D. Julius. 2008. Pungent agents from Szechuan peppers excite sensory neurons by inhibiting two-pore potassium channels. *Nat. Neurosci.* 11:772–779.
- Ben-Abu, Y., Y. Zhou, N. Zilberberg, and O. Yifrach. 2009. Inverse coupling in leak and voltage-activated K⁺ channel gates underlies distinct roles in electrical signaling. *Nat. Struct. Mol. Biol.* 16:71–79.
- Brelidze, T.I., X. Niu, and K.L. Magleby. 2003. A ring of eight conserved negatively charged amino acids doubles the conductance of BK channels and prevents inward rectification. *Proc. Natl. Acad. Sci. USA*. 100:9017–9022.
- Brooks, B.R., R.E. Brucolieri, B.D. Olafson, D.J. States, S. Swaminathan, and M. Karplus. 1983. CHARMM: a program for macromolecular energy, minimization, and dynamics calculations. *J. Comput. Chem.* 4:187–217.
- Canutescu, A.A., A.A. Shelenkov, and R.L. Dunbrack Jr. 2003. A graph-theory algorithm for rapid protein side-chain prediction. *Protein Sci.* 12:2001–2014.
- Carvacho, I., W. Gonzalez, Y.P. Torres, S. Brauchi, O. Alvarez, F.D. Gonzalez-Nilo, and R. Latorre. 2008. Intrinsic electrostatic potential in the BK channel pore: role in determining single channel conductance and block. *J. Gen. Physiol.* 131:147–161.
- Casamassima, M., M.C. D'Adamo, M. Pessia, and S.J. Tucker. 2003. Identification of a heteromeric interaction that influences the rectification, gating, and pH sensitivity of Kir4.1/Kir5.1 potassium channels. *J. Biol. Chem.* 278:43533–43540.
- Castellano, A., M.D. Chiara, B. Mellström, A. Molina, F. Monje, J.R. Naranjo, and J. López-Barneo. 1997. Identification and functional characterization of a K⁺ channel alpha-subunit with regulatory properties specific to brain. *J. Neurosci.* 17:4652–4661.
- Chatelain, F.C., N. Alagem, Q. Xu, R. Pancaroglu, E. Reuveny, and D.L. Minor Jr. 2005. The pore helix dipole has a minor role in inward rectifier channel function. *Neuron*. 47:833–843.
- Chen, H., and S.A.N. Goldstein. 2007. Serial perturbation of MinK in IKs implies an alpha-helical transmembrane span traversing the channel corpus. *Biophys. J.* 93:2332–2340.
- Collins, A., H. Chuang, Y.N. Jan, and L.Y. Jan. 1997. Scanning mutagenesis of the putative transmembrane segments of Kir2.1, an inward rectifier potassium channel. *Proc. Natl. Acad. Sci. USA*. 94:5456–5460.
- Cordero-Morales, J.F., L.G. Cuello, and E. Perozo. 2006. Voltage-dependent gating at the KcsA selectivity filter. *Nat. Struct. Mol. Biol.* 13:319–322.
- Cordero-Morales, J.F., V. Jogini, A. Lewis, V. Vásquez, D.M. Cortes, B. Roux, and E. Perozo. 2007. Molecular driving forces determining potassium channel slow inactivation. *Nat. Struct. Mol. Biol.* 14:1062–1069.
- Cymes, G.D., Y. Ni, and C. Grosman. 2005. Probing ion-channel pores one proton at a time. *Nature*. 438:975–980.
- Czirják, G., and P. Enyedi. 2002. Formation of functional heterodimers between the TASK-1 and TASK-3 two-pore domain potassium channel subunits. *J. Biol. Chem.* 277:5426–5432.
- Davies, L.A., C. Hu, N.A. Guagliardo, N. Sen, X. Chen, E.M. Talley, R.M. Carey, D.A. Bayliss, and P.Q. Barrett. 2008. TASK channel deletion in mice causes primary hyperaldosteronism. *Proc. Natl. Acad. Sci. USA*. 105:2203–2208.
- Doyle, D.A., J. Morais Cabral, R.A. Pfuetzner, A. Kuo, J.M. Gulbis, S.L. Cohen, B.T. Chait, and R. MacKinnon. 1998. The structure of the potassium channel: molecular basis of K⁺ conduction and selectivity. *Science*. 280:69–77.
- Duprat, F., F. Lesage, M. Fink, R. Reyes, C. Heurteaux, and M. Lazdunski. 1997. TASK, a human background K⁺ channel to sense external pH variations near physiological pH. *EMBO J.* 16:5464–5471.
- Fink, M., F. Duprat, F. Lesage, R. Reyes, G. Romey, C. Heurteaux, and M. Lazdunski. 1996. Cloning, functional expression and brain localization of a novel unconventional outward rectifier K⁺ channel. *EMBO J.* 15:6854–6862.
- Fiser, A., and A. Sali. 2003. ModLoop: automated modeling of loops in protein structures. *Bioinformatics*. 19:2500–2501.
- Gilson, M.K., and B.H. Honig. 1986. The dielectric constant of a folded protein. *Biopolymers*. 25:2097–2119.
- Goldstein, S.A.N., L.A. Price, D.N. Rosenthal, and M.H. Pausch. 1996. ORK1, a potassium-selective leak channel with two pore domains cloned from *Drosophila melanogaster* by expression in *Saccharomyces cerevisiae*. *Proc. Natl. Acad. Sci. USA*. 93:13256–13261.
- Goldstein, S.A.N., D. Bockenhauer, I. O'Kelly, and N. Zilberberg. 2001. Potassium leak channels and the KCNK family of two-P-domain subunits. *Nat. Rev. Neurosci.* 2:175–184.
- Hidalgo, P., and R. MacKinnon. 1995. Revealing the architecture of a K⁺ channel pore through mutant cycles with a peptide inhibitor. *Science*. 268:307–310.
- Higgins, D.G., J.D. Thompson, and T.J. Gibson. 1996. Using CLUSTAL for multiple sequence alignments. *Methods Enzymol.* 266:383–402.
- Honig, B., and A. Nicholls. 1995. Classical electrostatics in biology and chemistry. *Science*. 268:1144–1149.
- Ilan, N., and S.A.N. Goldstein. 2001. Kcnk0: single, cloned potassium leak channels are multi-ion pores. *Biophys. J.* 80:241–253.
- Im, W., D. Beglov, and B. Roux. 1998. Continuum solvation model: computation of electrostatic forces from numerical solutions to the Poisson-Boltzmann equation. *Comput. Phys. Commun.* 111:59–75.

- Jiang, Y., A. Lee, J. Chen, M. Cadene, B.T. Chait, and R. MacKinnon. 2002. Crystal structure and mechanism of a calcium-gated potassium channel. *Nature*. 417:515–522.
- Jiang, Y., A. Lee, J.Y. Chen, V. Ruta, M. Cadene, B.T. Chait, and R. MacKinnon. 2003. X-ray structure of a voltage-dependent K⁺ channel. *Nature*. 423:33–41.
- Jogini, V., and B. Roux. 2005. Electrostatics of the intracellular vestibule of K⁺ channels. *J. Mol. Biol.* 354:272–288.
- Ketchum, K.A., W.J. Joiner, A.J. Sellers, L.K. Kaczmarek, and S.A.N. Goldstein. 1995. A new family of outwardly rectifying potassium channel proteins with two pore domains in tandem. *Nature*. 376:690–695.
- King, G., F.S. Lee, and A. Warshel. 1991. Microscopic simulations of macroscopic dielectric constants of solvated proteins. *J. Chem. Phys.* 95:4366–4377.
- Kuo, A., J.M. Gulbis, J.F. Antcliff, T. Rahman, E.D. Lowe, J. Zimmer, J. Cuthbertson, F.M. Ashcroft, T. Ezaki, and D.A. Doyle. 2003. Crystal structure of the potassium channel KirBac1.1 in the closed state. *Science*. 300:1922–1926.
- Lalevée, N., B. Monier, S. Sénatore, L. Perrin, and M. Sémeriva. 2006. Control of cardiac rhythm by ORK1, a *Drosophila* two-pore domain potassium channel. *Curr. Biol.* 16:1502–1508.
- Lesage, F., M. Mattéi, M. Fink, J. Barhanin, and M. Lazdunski. 1996. Assignment of the human weak inward rectifier K⁺ channel TWIK-1 gene to chromosome 1q42-q43. *Genomics*. 34:153–155.
- Li, L., I. Vorob'ev, A.D. MacKerell Jr., and T.W. Allen. 2008. Is arginine charged in a membrane? *Biophys. J.* 94:L11–L13.
- Long, S.B., E.B. Campbell, and R. MacKinnon. 2005. Crystal structure of a mammalian voltage-dependent Shaker family K⁺ channel. *Science*. 309:897–903.
- Lopes, C.M.B., P.G. Gallagher, M.E. Buck, M.H. Butler, and S.A.N. Goldstein. 2000. Proton block and voltage gating are potassium-dependent in the cardiac leak channel Kcnk3. *J. Biol. Chem.* 275:16969–16978.
- Lopes, C.M.B., N. Zilberman, and S.A.N. Goldstein. 2001. Block of Kcnk3 by protons. Evidence that 2-P-domain potassium channel subunits function as homodimers. *J. Biol. Chem.* 276:24449–24452.
- Lotshaw, D.P. 2007. Biophysical, pharmacological, and functional characteristics of cloned and native mammalian two-pore domain K⁺ channels. *Cell Biochem. Biophys.* 47:209–256.
- MacKerell, A.D., D. Bashford, M. Bellott, R.L. Dunbrack, J.D. Evanseck, M.J. Field, S. Fischer, J. Gao, H. Guo, S. Ha, et al. 1998. All-atom empirical potential for molecular modeling and dynamics studies of proteins. *J. Phys. Chem. B.* 102:3586–3616.
- MacKinnon, R. 1991. Determination of the subunit stoichiometry of a voltage-activated potassium channel. *Nature*. 350:232–235.
- Mulkey, D.K., E.M. Talley, R.L. Stornetta, A.R. Siegel, G.H. West, X. Chen, N. Sen, A.M. Mistry, P.G. Guyenet, and D.A. Bayliss. 2007. TASK channels determine pH sensitivity in select respiratory neurons but do not contribute to central respiratory chemosensitivity. *J. Neurosci.* 27:14049–14058.
- Niemeyer, M.I., F.D. González-Nilo, L. Zúñiga, W. González, L.P. Cid, and F.V. Sepúlveda. 2007. Neutralization of a single arginine residue gates open a two-pore domain, alkali-activated K⁺ channel. *Proc. Natl. Acad. Sci. USA*. 104:666–671.
- Nimigean, C.M., J.S. Chappie, and C. Miller. 2003. Electrostatic tuning of ion conductance in potassium channels. *Biochemistry*. 42:9263–9268.
- Nina, M., D. Beglov, and B. Roux. 1997. Atomic radii for continuum electrostatics calculations based on molecular dynamics free energy simulations. *J. Phys. Chem. B.* 101:5239–5248.
- Ranganathan, R., J.H. Lewis, and R. MacKinnon. 1996. Spatial localization of the K⁺ channel selectivity filter by mutant cycle-based structure analysis. *Neuron*. 16:131–139.
- Roller, A., G. Natura, H. Bihler, C.L. Slayman, C. Eing, and A. Bertl. 2005. In the yeast potassium channel, Tok1p, the external ring of aspartate residues modulates both gating and conductance. *Pflügers Arch.* 451:362–370.
- Rosenhouse-Dantsker, A., and D.E. Logothetis. 2007. Potassium channel gating in the absence of the highly conserved glycine of the inner transmembrane helix. *Channels (Austin)*. 1:189–197.
- Roux, B. 1997. Influence of the membrane potential on the free energy of an intrinsic protein. *Biophys. J.* 73:2980–2989.
- Roux, B. 2005. The art of dissecting the function of a potassium channel. *Neuron*. 47:777–778.
- Roux, B., and R. MacKinnon. 1999. The cavity and pore helices in the KcsA K⁺ channel: electrostatic stabilization of monovalent cations. *Science*. 285:100–102.
- Roux, B., and K. Schulten. 2004. Computational studies of membrane channels. *Structure*. 12:1343–1351.
- Roux, B., S. Bernèche, and W. Im. 2000. Ion channels, permeation, and electrostatics: insight into the function of KcsA. *Biochemistry*. 39:13295–13306.
- Schutz, C.N., and A. Warshel. 2001. What are the dielectric “constants” of proteins and how to validate electrostatic models? *Proteins: Structure, Function, and Bioinformatics*. 44:400–417.
- Simonson, T., and C.L. Brooks III. 1996. Charge screening and the dielectric constant of proteins: insights from molecular dynamics. *J. Am. Chem. Soc.* 118:8452–8458.
- Simonson, T., and D. Perahia. 1995. Microscopic dielectric properties of cytochrome c from molecular dynamics simulations in aqueous solution. *J. Am. Chem. Soc.* 117:7987–8000.
- Stansfeld, P.J., A. Grottesi, Z.A. Sands, M.S. Sansom, P. Geddeck, M. Gosling, B. Cox, P.R. Stanfield, J.S. Mitcheson, and M.J. Sutcliffe. 2008. Insight into the mechanism of inactivation and pH sensitivity in potassium channels from molecular dynamics simulations. *Biochemistry*. 47:7414–7422.
- Thomas, D., and S.A.N. Goldstein. 2009. Structure and function of ion channels: two-P-domain (K_{2P}) potassium channels: leak conductance regulators of excitability. In *Encyclopedia of Neuroscience*. L.R. Squire, T. Albright, F. Gage, N. Spitzer, and F. Bloom, editors. Elsevier, Boston. 1207–1220.
- Thomas, D., L.D. Plant, C.M. Wilkens, Z.A. McCrossan, and S.A.N. Goldstein. 2008. Alternative translation initiation in rat brain yields K2P2.1 potassium channels permeable to sodium. *Neuron*. 58:859–870.
- Tiwari-Woodruff, S.K., C.T. Schulteis, A.F. Mock, and D.M. Papazian. 1997. Electrostatic interactions between transmembrane segments mediate folding of Shaker K⁺ channel subunits. *Biophys. J.* 72:1489–1500.
- Tiwari-Woodruff, S.K., M-c.A. Lin, C.T. Schulteis, and D.M. Papazian. 2000. Voltage-dependent structural interactions in the Shaker K⁺ channel. *J. Gen. Physiol.* 115:123–138.
- White, S.H., and M.C. Wiener. 1996. The liquid-crystallographic structure of fluid lipid bilayer membranes. In *Biological Membranes: a Molecular Perspective from Computation and Experiment*. Vol. 1. K.J. Merz Jr. and B. Roux, editors. Birkhauser, Boston. 127–144.
- Yuill, K.H., P.J. Stansfeld, I. Ashmole, M.J. Sutcliffe, and P.R. Stanfield. 2007. The selectivity, voltage-dependence and acid sensitivity of the tandem pore potassium channel TASK-1: contributions of the pore domains. *Pflügers Arch.* 455:333–348.
- Zhou, Y., J.H. Morais-Cabral, A. Kaufman, and R. MacKinnon. 2001. Chemistry of ion coordination and hydration revealed by a K⁺ channel-Fab complex at 2.0 Å resolution. *Nature*. 414:43–48.
- Zilberman, N., N. Ilan, R. Gonzalez-Colaso, and S.A.N. Goldstein. 2000. Opening and closing of KCNKO potassium leak channels is tightly regulated. *J. Gen. Physiol.* 116:721–734.
- Zilberman, N., N. Ilan, and S.A. Goldstein. 2001. KCNKØ: opening and closing the 2-P-domain potassium leak channel entails “C-type” gating of the outer pore. *Neuron*. 32:635–648.

Kollewe et al., <http://www.jgp.org/cgi/content/full/jgp.200910235/DC1>

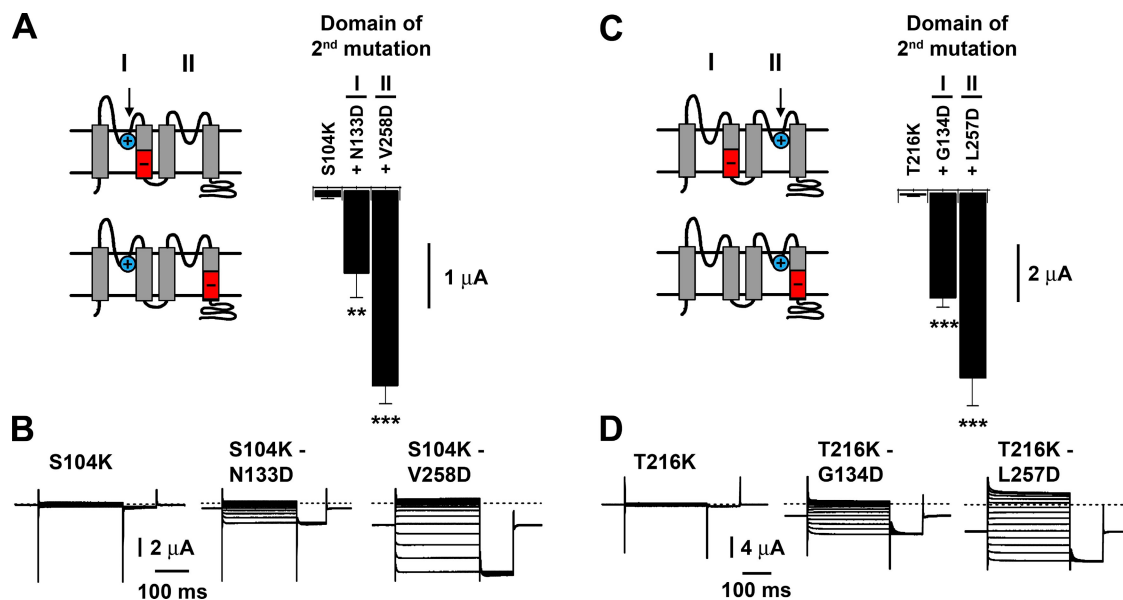


Figure S1. Restoration of function by second site changes in full-length K_{2P}Ø channels. Currents were studied as in Fig. 2 A. Bar graphs show current amplitude \pm SEM at -100 mV. Topology insets: blue circles denote full-length K_{2P}Ø channels with S104K in P1 or T216K in P2, and red bars indicate the sites in TM2 or TM4 altered to aspartate. (A) S104K K_{2P}Ø channels with no other change or second sites altered to aspartate in TM2 or TM4. Statistical differences versus S104K are indicated ($n = 8-10$). (B) Sample current traces for channels in A in which second mutations show different restoring effectiveness. (C) T216K K_{2P}Ø channels with no other change or second sites altered to aspartate in TM2 or TM4. Statistical differences versus T216K are indicated ($n = 3-4$). (D) Sample current traces for channels in C in which second mutations show different restoring effectiveness. **, $P < 0.01$; ***, $P < 0.001$.

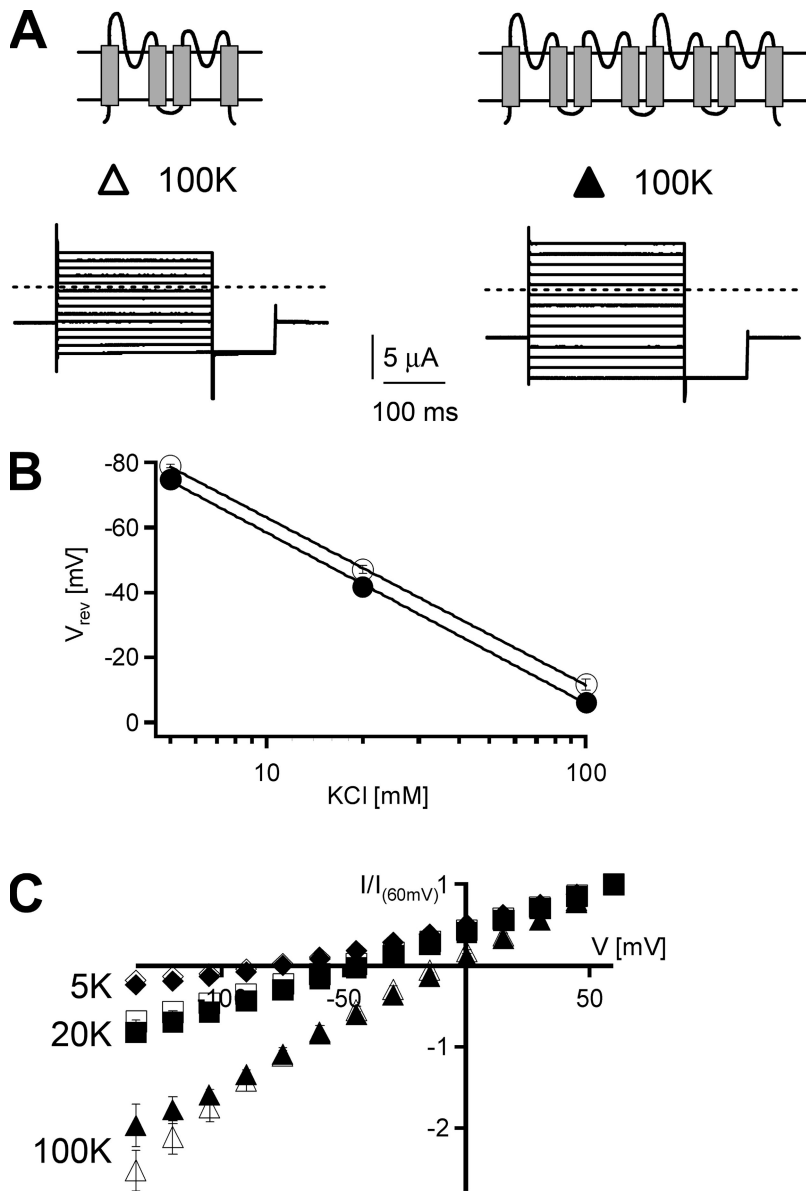


Figure S2. Comparison of $\Delta\text{K}_{2\text{P}}\emptyset$ channels formed by monomeric subunits or tandem dimer constructs. Currents were studied as in Fig. 2 A. (A) Predicted topology of $\Delta\text{K}_{2\text{P}}\emptyset$ (left) or $\Delta\text{K}_{2\text{P}}\emptyset-\Delta\text{K}_{2\text{P}}\emptyset$ (right) subunits. (B) Channels formed by $\Delta\text{K}_{2\text{P}}\emptyset$ (open circles) or $\Delta\text{K}_{2\text{P}}\emptyset-\Delta\text{K}_{2\text{P}}\emptyset$ (closed circles) subunits are potassium selective. Reversal potentials ($\pm\text{SEM}$; $n = 3-5$) were determined in bath solutions containing 5, 20, or 100 mM KCl as in Fig. 2 A. Linear regression shows a shift of 52 ± 1 mV for $\Delta\text{K}_{2\text{P}}\emptyset$ and 53 ± 1 mV for $\Delta\text{K}_{2\text{P}}\emptyset-\Delta\text{K}_{2\text{P}}\emptyset$ channels with a 10-fold change in potassium concentration. KCl was isotonically replaced for NaCl in solutions that contained 5 or 20 mM KCl. (C) Current-voltage relationships of $\Delta\text{K}_{2\text{P}}\emptyset$ (open symbols) or $\Delta\text{K}_{2\text{P}}\emptyset-\Delta\text{K}_{2\text{P}}\emptyset$ (closed symbols) channels with 5 (diamonds), 20 (squares), or 100 mM (triangles) KCl in the bath solution normalized to the current at 60 mV ($n = 3-5$).

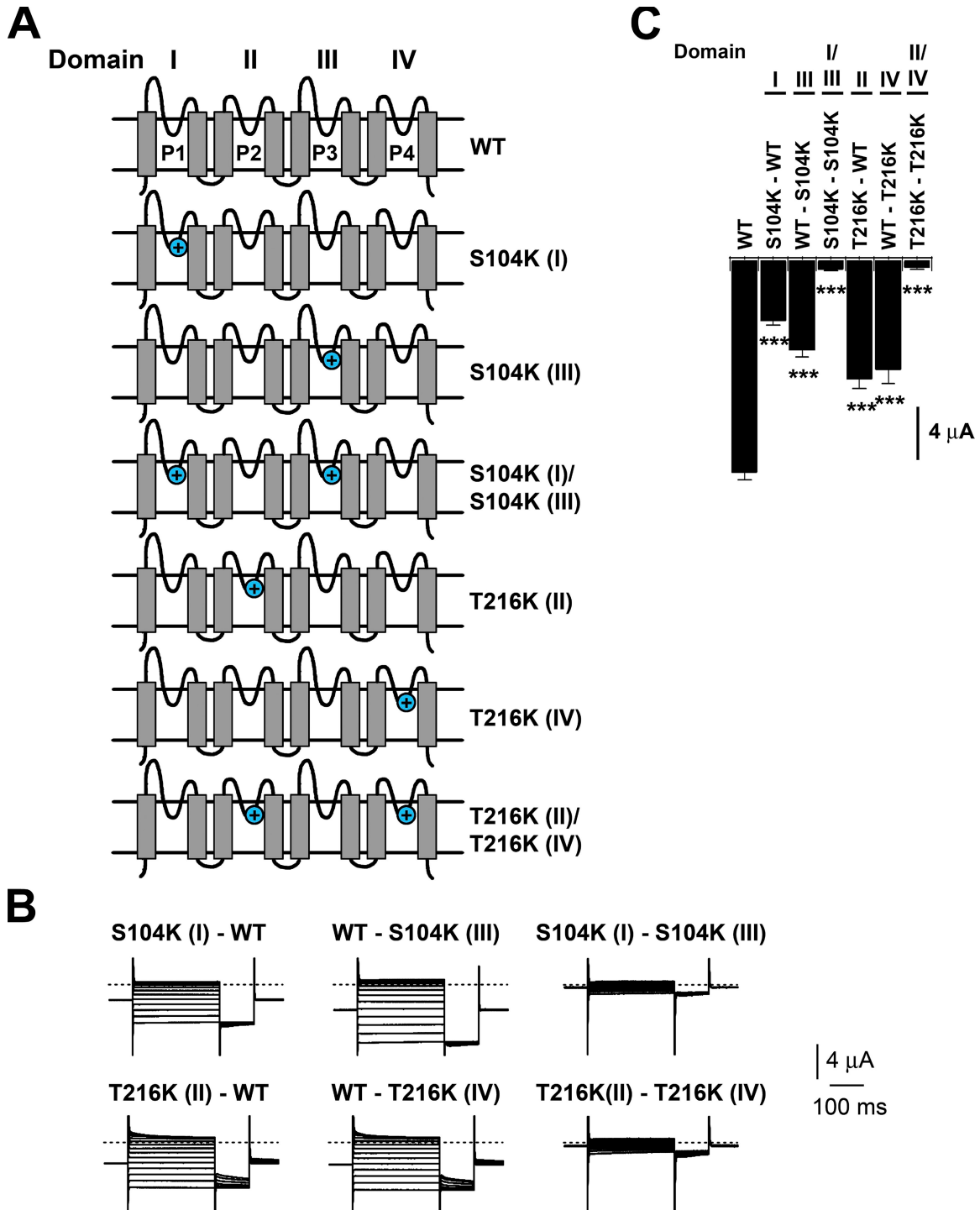


Figure S3. All four P domains of $\Delta K_{2p}\emptyset-\Delta K_{2p}\emptyset$ subunits contribute to the pore. Currents were studied as in Fig. 2 A. (A) Schematic of $\Delta K_{2p}\emptyset-\Delta K_{2p}\emptyset$ channels with S104K in domain I and/or domain III, or T216K in domain II and/or domain IV indicated by blue circles. (B) Representative currents from selected $\Delta K_{2p}\emptyset-\Delta K_{2p}\emptyset$ channels as indicated. (C) Currents \pm SEM at -100 mV from oocytes expressing WT $\Delta K_{2p}\emptyset-\Delta K_{2p}\emptyset$ channels or mutants as indicated. Statistical differences from WT $\Delta K_{2p}\emptyset-\Delta K_{2p}\emptyset$ channels ($n = 5-15$) are shown. ***, $P < 0.001$.

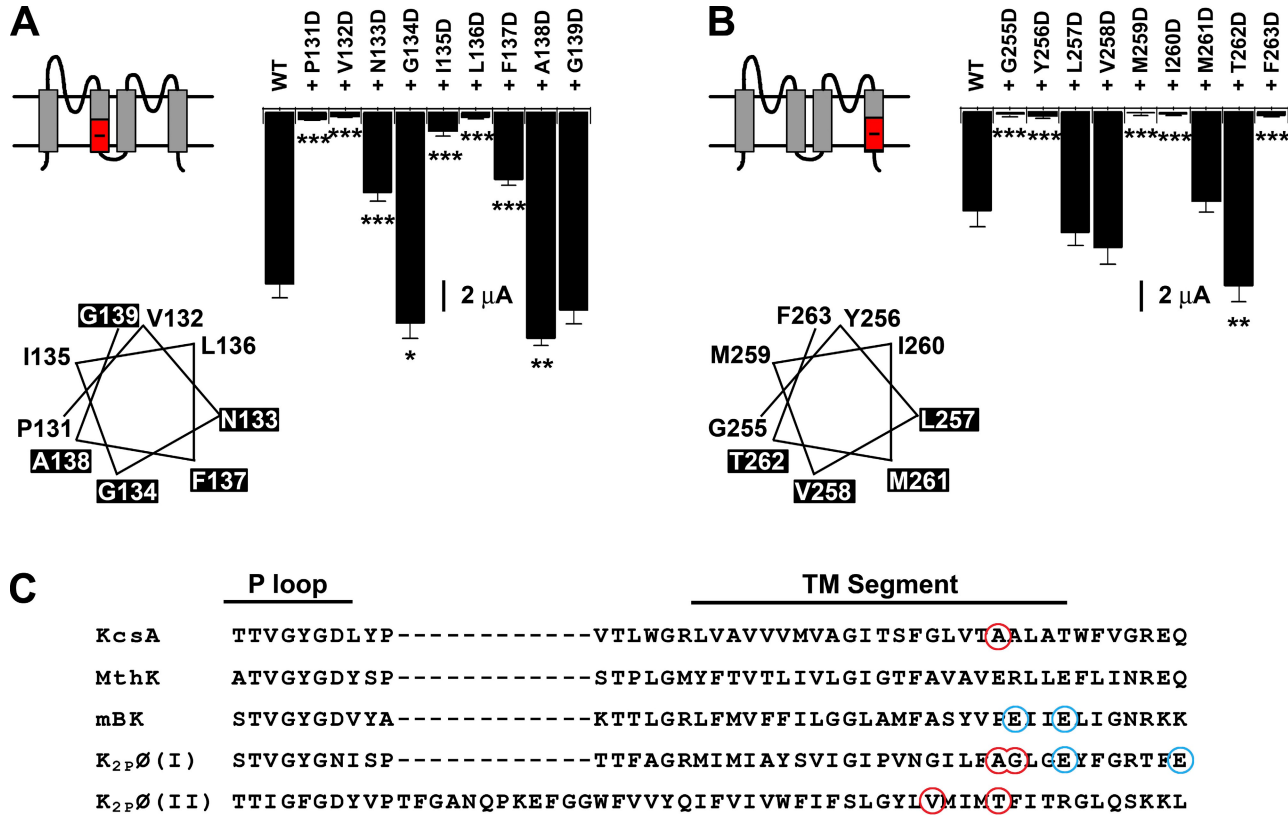


Figure S4. Tolerance of TM2 and TM4 sites for aspartate substitution. Currents were studied as in Fig. 2 A. Bar graphs plot current amplitudes \pm SEM at -100 mV. Statistical differences versus WT $\Delta K_{2P}\emptyset$ channels. (A) WT $\Delta K_{2P}\emptyset$ or channels with sites altered to aspartate from positions 131 to 139 in TM2. The red box indicates TM2 sites serially altered to aspartate ($n = 10$). A helical wheel plot indicates five TM2 sites that can be mutated without disruption of channel function with black shading (133, 134, 137, 138, and 139). (B) WT $\Delta K_{2P}\emptyset$ or channels with sites altered to aspartate from positions 255 to 263 in TM4. The red box indicates TM4 sites serially altered to aspartate ($n = 6$ –13). A helical wheel plot indicates four TM4 sites that can be mutated without disruption of channel function with black shading (257, 258, 261, and 262). (C) Alignment of KcsA (amino acids 74–119), MthK (amino acids 58–103), mBK (amino acids 351–396), $K_{2P}\emptyset$ P1 and TM2 (amino acids 104–149), and $K_{2P}\emptyset$ P2 and TM4 (amino acids 216–273) using ClustalW. P loops and predicted TM spans are marked with black lines. Neutralization of glutamates circled in blue reduces single-channel conductance. Aspartate substitution of residues circled in red increases single-channel conductance (for $K_{2P}\emptyset$, this is after neutralization of the glutamate residues circled in blue). *, $P < 0.05$; **, $P < 0.01$; ***, $P < 0.001$.

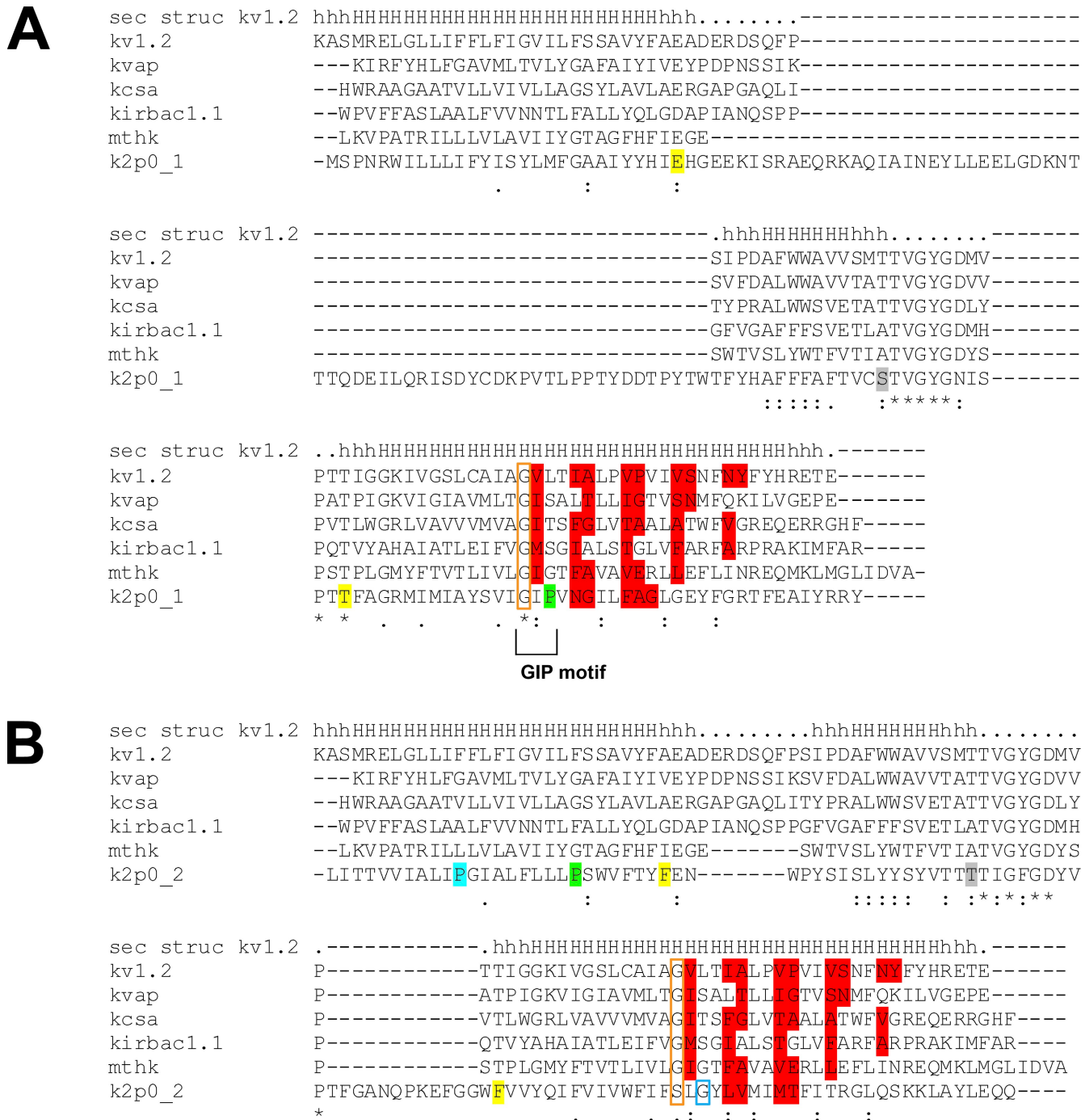


Figure S5. Alignment of $K_{2p}\emptyset$ with channels of known crystal structure. Alignment of $K_v1.2$ TM5-P-TM6 (amino acids 322–422) with $K_{2p}\emptyset$ using ClustalW (Higgins et al. 1996. *Methods Enzymol.* 266:383–402) and including the homologous segments of the crystallized potassium channels K_v AP (amino acids 160–257), KcsA (amino acids 25–125), K_{ii} Bac1.1 (amino acids 60–160), and MthK (amino acids 16–113). Alignment was enhanced based on $K_{2p}\emptyset$ positions predicted to be exposed to the aqueous pore. (top row) Secondary structure of $K_v1.2$. H denotes the α -helix; dots denote random coils. Yellow, residues that can form a disulfide bridge when mutated to cysteines (E28C–T115C and F199C–F239C). Green, proline residues 131 and 192, which are present in TM segments of several K_{2p} channels. Blue, proline 183, which is not conserved. Red, residues shown to be pore exposed in $K_v1.2$ (Long et al. 2005. *Science*. 309:897–903), KcsA (Doyle et al. 1998. *Science*. 280:69–77), K_{ii} Bac1.1 (Kuo et al. 2003. *Science*. 300:1922–1926), MthK (Jiang et al. 2002. *Nature*. 417:523–526), or K_v AP (Jiang et al. 2003. *Nature*. 423:33–41) or predicted to be pore exposed in $K_{2p}\emptyset$. Gray, S104 and T216 of $K_{2p}\emptyset$. Orange box, glycine residues in the position of the glycine hinge identified in MthK. Blue box, glycine conserved in TM4 of all K_{2p} channels. The GIP motif in TM2 is indicated. Asterisks mark identical amino acids; double dots mark conserved amino acids; single dots mark semiconserved amino acids. (A) Alignment with $K_{2p}\emptyset$ TM1-P1-TM2 (amino acids 1–155). (B) Alignment with $K_{2p}\emptyset$ TM3-P2-TM4 (amino acids 173–279).

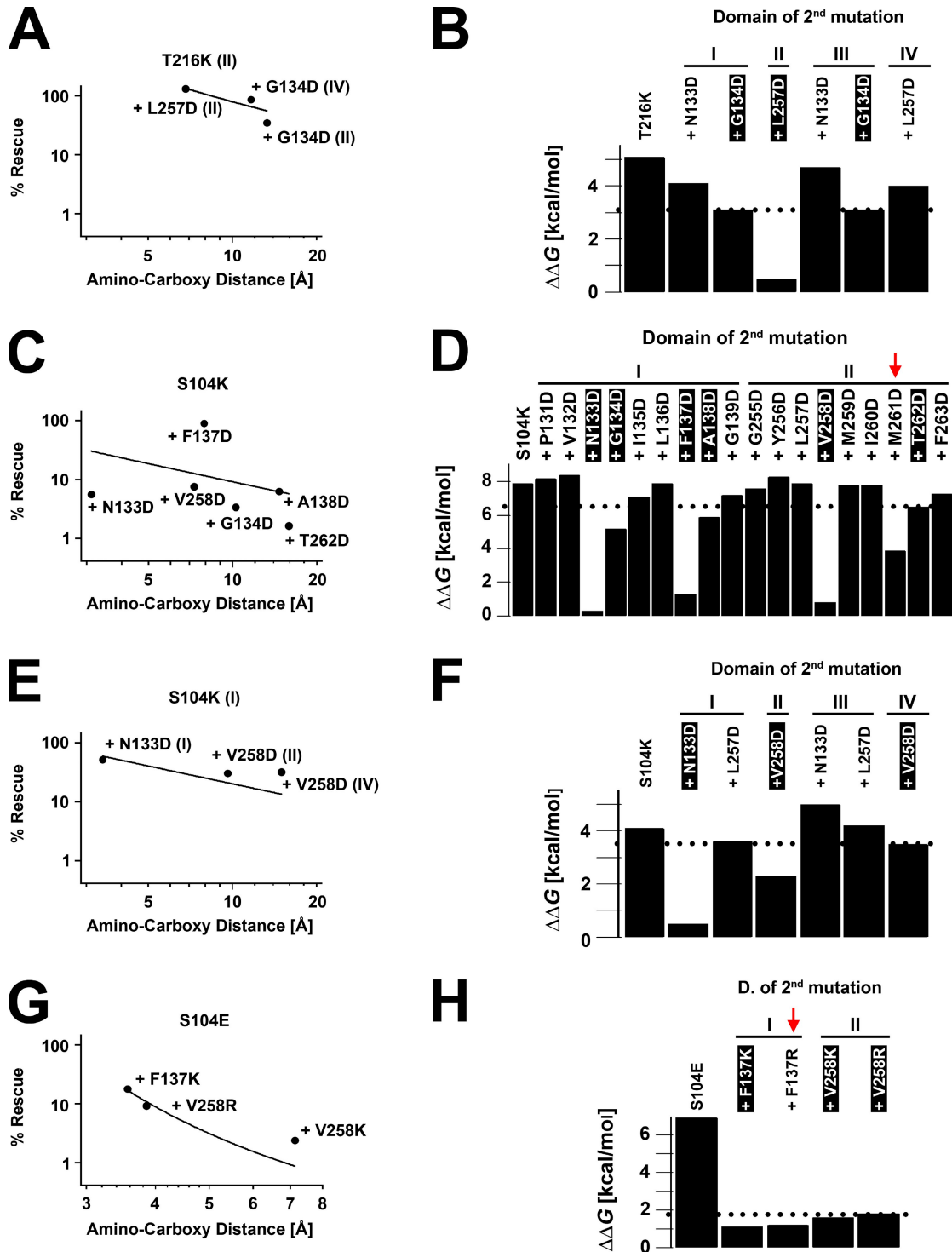
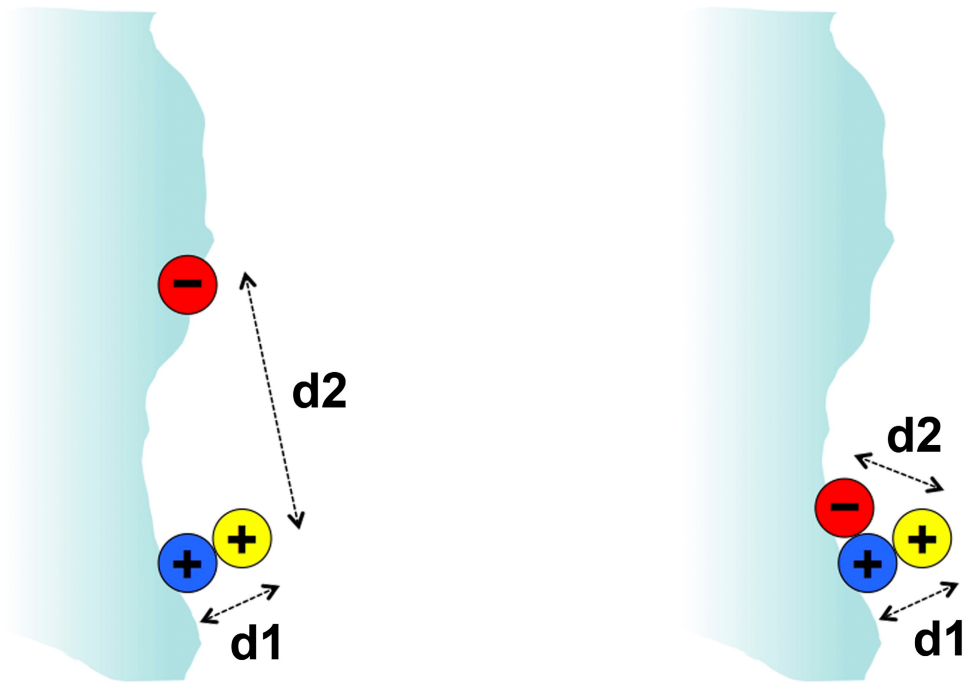


Figure S6. Electrostatic calculations based on the refined twofold symmetric model. Effectiveness of complementation as a function of distance between the ϵ -amino and carboxylate carbon atoms in the $\Delta K_{2p}\emptyset$ channel mutants. Rescue percentage was determined at -100 mV as $(I_{\text{double mutant}} - I_{\text{single mutant}})/(I_{\text{WT}} - I_{\text{single mutant}})$. Distances were measured as in Table I. Data were fit to $f(x) = a(e^{bx} - 1)$. Electrostatic $\Delta\Delta G$ (static field contribution) with respect to WT $\Delta K_{2p}\emptyset$ for a potassium ion entering the channel from the cytoplasm. The highest $\Delta\Delta G$ level at which rescue was observed is marked with a black dotted line. Atomic charges were turned off in the calculations in the following positions: 30–91, 153–173, 225–238, side chain and carbonyl groups of 105 and 217, and main chain of 106–109 and 218–221. Black shading indicates mutations that restored current. Red arrows mark mismatches between experimental and computational results for rescue. (A) Complementation effectiveness in T216K (II) tandem channels. (B) $\Delta\Delta G$ (static field contribution) with respect to WT $\Delta K_{2p}\emptyset$ for channels in A. (C) Complementation effectiveness in S104K channels. (D) $\Delta\Delta G$ (static field contribution) with respect to WT $\Delta K_{2p}\emptyset$ for channels in C. (E) Complementation effectiveness in S104K (I) tandem channels. (F) $\Delta\Delta G$ (static field contribution) with respect to WT $\Delta K_{2p}\emptyset$ for channels in E. (G) Complementation effectiveness in S104E channels. (H) $\Delta\Delta G$ (static field contribution) with respect to WT $\Delta K_{2p}\emptyset$ for channels in G.



ion (yellow) is at distance d_1 from the positively charged residue (blue) and that their unfavorable interaction is $E_1 = Q_1 \times Q_{\text{ion}} / (\epsilon \times d_1)$, where ϵ is some effective dielectric constant. A negatively charged residue (red) introduced elsewhere in the channel at distance d_2 from the permeating ion causes a favorable electrostatic interaction: $E_2 = Q_2 \times Q_{\text{ion}} / (\epsilon \times d_2)$. The two residues have opposite charges, $Q_2 = -Q_1$, which leads to the simple relation $E_2 = -E_1 (d_1/d_2)$. It is reasonable to assume that d_2 roughly mirrors the separation between the two mutations and can vary from a distance of d_1 (where compensation occurs) up to larger distances where compensation does not occur. The rescue of ionic current is defined as $\text{Rescue} = [I(\text{double}) - I(\text{single})] / [I(\text{WT}) - I(\text{single})]$, where $I(\text{WT})$, $I(\text{single})$, and $I(\text{double})$ are the currents observed in the WT, single, and double mutants, respectively. Let us assume that the main effect of the single and double mutants on the current can be expressed simply as $I(\text{single}) = I(\text{WT}) \times \exp(-E_1/kT)$ and $I(\text{double}) = I(\text{WT}) \times \exp(-(E_1 + E_2)/kT)$. Then, this leads to the equation $\text{Rescue} = [\exp(-(E_1 + E_2)/kT) - \exp(-E_1/kT)] / [1.0 - \exp(-E_1/kT)]$. This equation was used to fit the data in Fig. 7 I and Fig. S6. E_1 and d_1 are the free parameters, and d_2 is taken as the distance between the two mutated residues from the three-dimensional model.

Figure S7. Schematic illustration of the mechanism of electrostatic compensation. The permeating potassium ion is shown in yellow. A first mutation (blue) inhibits the ionic current by introducing a large energy barrier along the permeation pathway. The largest effect from this unfavorable mutation occurs when the permeating ion is near the positively charged residue. A second mutation (red) of opposite charge is introduced at different positions to try to restore the ionic current. On the left, the mutation is introduced far away from the first mutation, and compensation does not occur. On the right, the two oppositely charged residues are in physical proximity, and their effects on the permeating ion cancel out. A simple model to explain the mechanism of electrostatic compensation: let us assume that in this situation, the

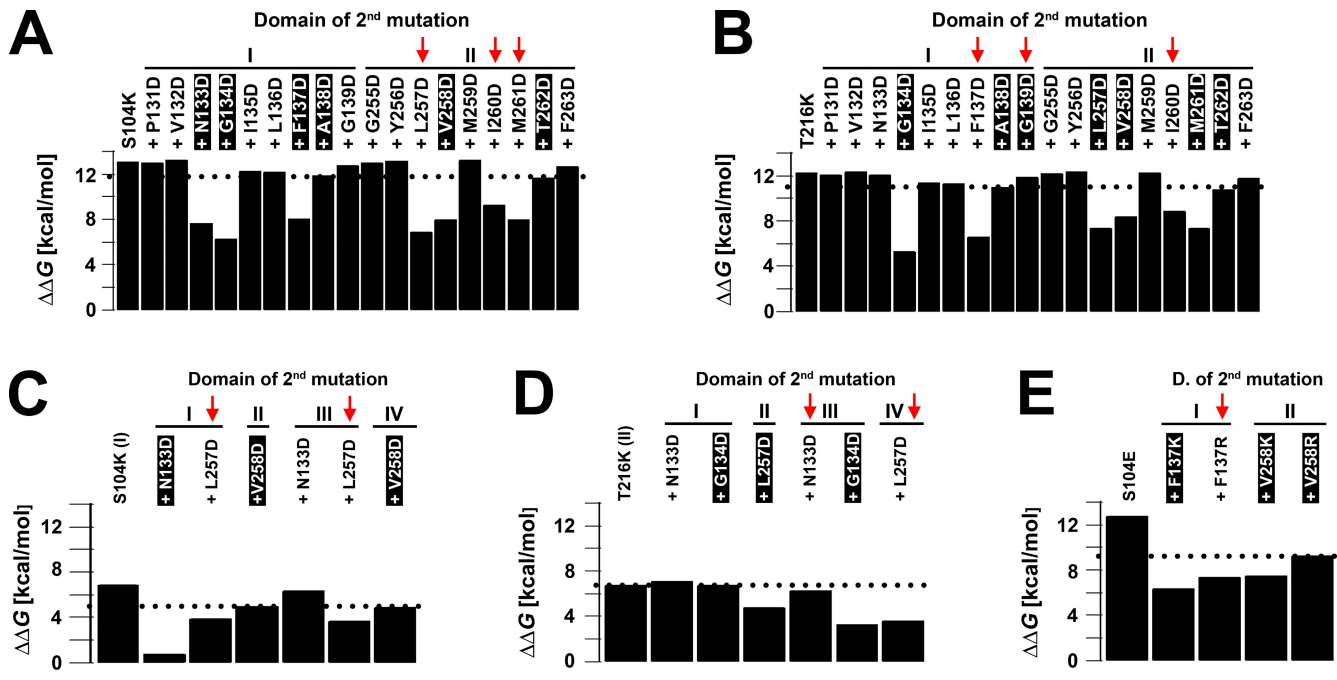


Figure S8. Electrostatic calculations based on the fourfold symmetric model. Electrostatic $\Delta\Delta G$ (static field contribution) for S104K (A), T216K (B), S104K (I) tandem (C), T216K (II) tandem (D), or S104E (E) channels with respect to WT $\Delta K_{2p}\emptyset$ for a potassium ion entering the channel from the cytoplasm. The highest $\Delta\Delta G$ level at which rescue was observed is marked with a black dotted line. Atomic charges were turned off in the calculations in the following positions: 30–91, 153–173, 225–238, side chain and carbonyl groups of 105 and 217, and main chain of 106–109 and 218–221. Black shading indicates mutations that restored current. Red arrows mark 11 mismatches between experimental and computational results for rescue.

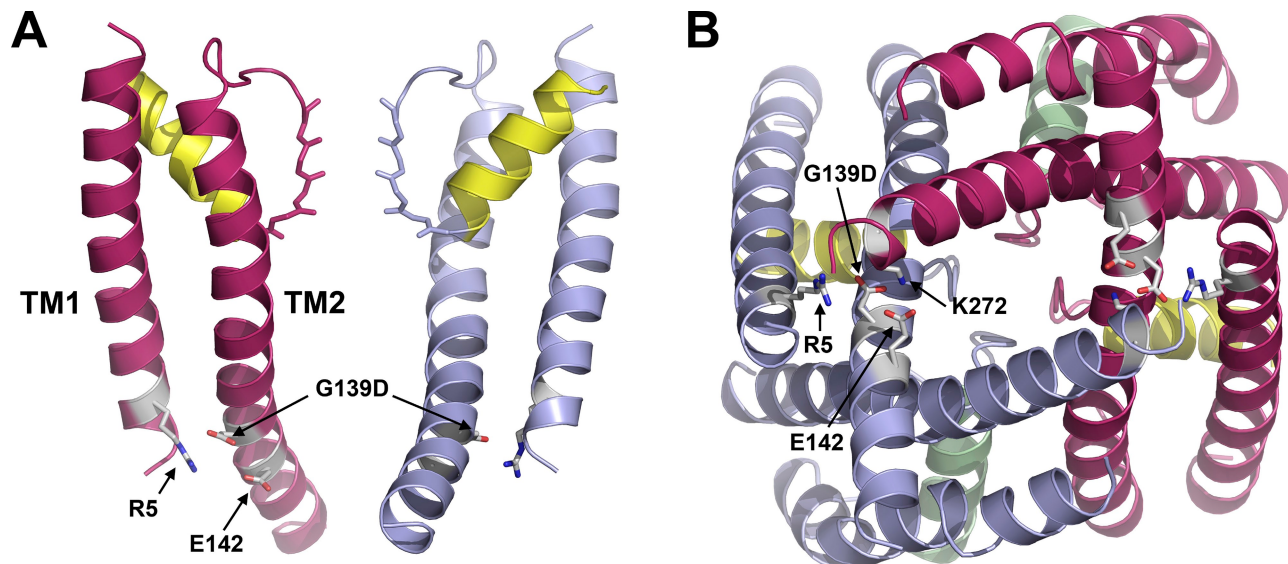


Figure S9. G139D is not in proximity to T216K in the $K_{2p}\emptyset$ model. G139D complements T216K but is near R5 in TM1, E142 in TM2, and K272 in TM4. It is seen to point away from the ion conduction pore and toward the perimembranous aqueous milieu, suggesting it does not interact with the suppressive pore lysine via a direct electrostatic mechanism. (A) Side view of domain I of the two subunits. Not depicted is T216K, which is positioned in domain II and is therefore not in the plane of the image. (B) Bottom view.

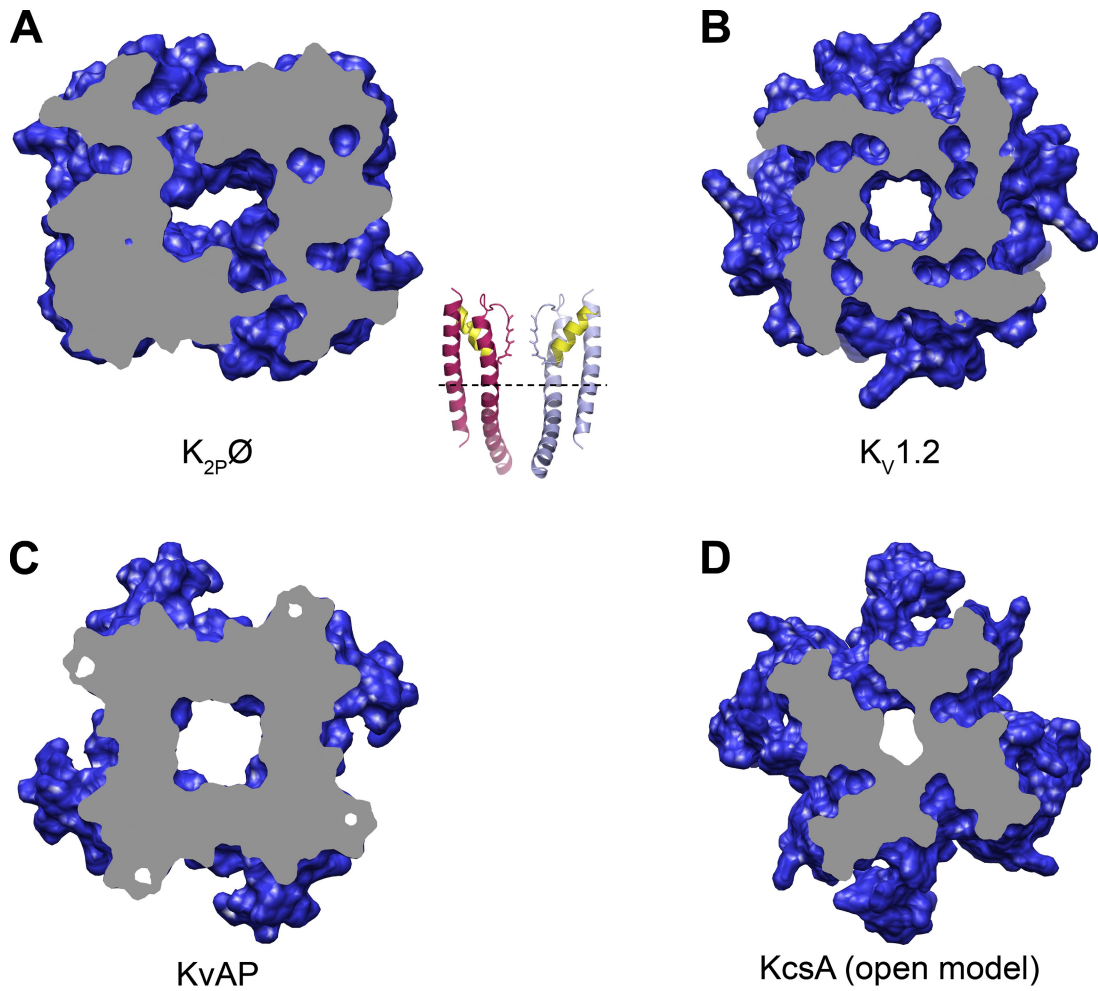


Figure S10. Cross section through the cavity of various potassium channels. Bottom view $\sim 4 \text{ \AA}$ below conserved threonine residues found in the selectivity filter of potassium channels (T105 and T217 in $K_{2P}\emptyset$ as shown in the inset in A). (A) $K_{2P}\emptyset$ model. (B) K_v AP (Jiang et al. 2003. *Nature*. 423:33–41). (C) K_v 1.2 (Long et al. 2005. *Science*. 309:897–903). (D) Open channel model of K_{cs} A based on the crystal structure of MthK (Jogini and Roux. 2005. *J. Mol. Biol.* 354:272–288).

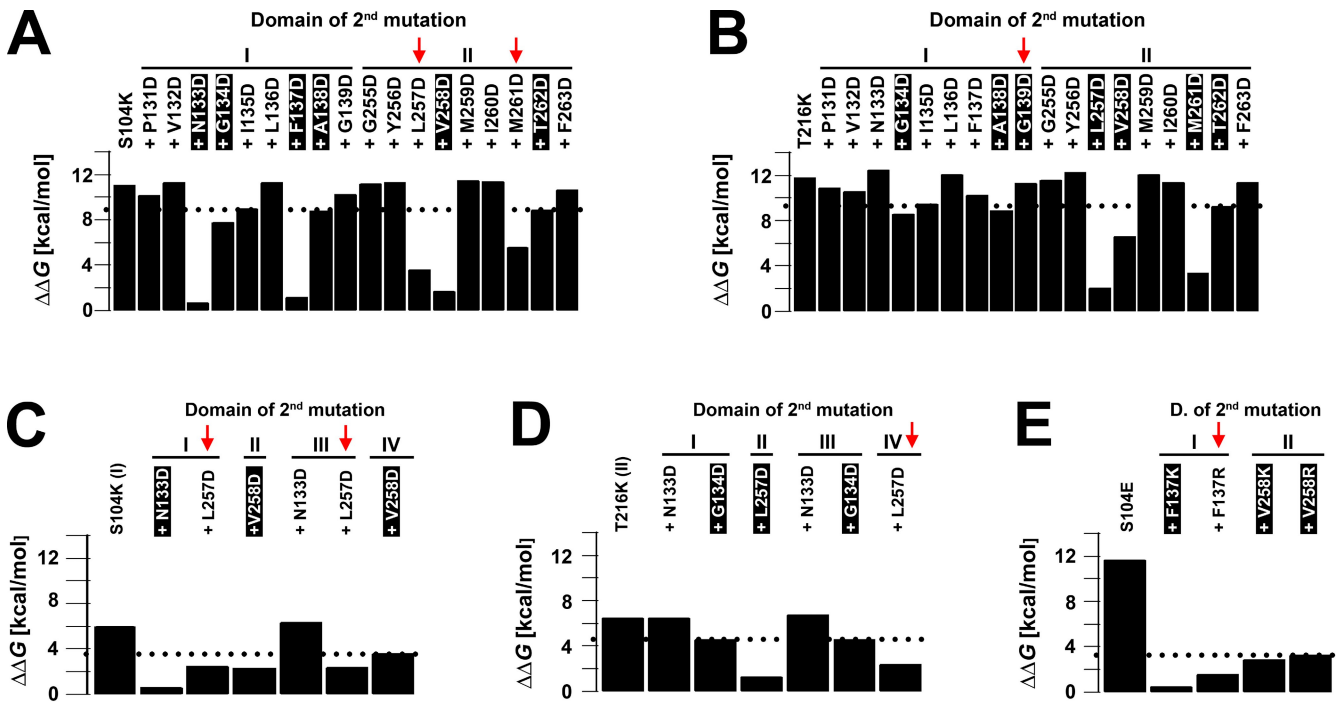


Figure S11. Electrostatic calculations based on twofold symmetric model before refinement. Electrostatic $\Delta\Delta G$ (static field contribution) for S104K (A), T216K (B), S104K (I) tandem (C), T216K (II) tandem (D), or S104E (E) channels with respect to WT $\Delta K_{2p}\emptyset$ for a potassium ion entering the channel from the cytoplasm. The highest $\Delta\Delta G$ level at which rescue was observed is marked with a black dotted line. Atomic charges were turned off in the calculations in the following positions: 30–91, 153–173, 225–238, side chain and carbonyl groups of 105 and 217, and main chain of 106–109 and 218–221. Black shading indicates mutations that restored current. Red arrows mark seven mismatches between experimental and computational results for rescue.